R & M No. 3818

R &M No. 3818

PROCUREMENT EXECUTIVE, MINISTRY OF DEFENCE

Aeronautical Research Council
Reports and Memoranda

ANALYSIS OF THE ZERO-LIFT WAVE DRAG MEASURED ON DELTA WINGS

by

J. Weber and C. King

London: Her Majesty's Stationery Office
1978

PRICE £6 NET

ANALYSIS OF THE ZERO-LIFT WAVE DRAG MEASURED ON DELTA WINGS*

By J. Weber** and C. King***

Reports and Memoranda No.3818****

June 1976

SUMMARY

An analysis is presented of measurements made at RAE in 1957-1959 on a series of delta wings. Lift and drag have been measured by strain-gauge balance at Mach numbers between 1.4 and 2.8. On some of the wings surface pressure distributions have also been measured. This Report deals mainly with the zero-lift wave drag, but also gives information on skin friction drag and lift-dependent drag. The wave drag has been obtained by integrating the pressure distribution. Values of the wave drag have also been derived from the measured total drag by subtracting estimated values for the skin-friction drag and for the effect of the sting support. The experimental values are compared with one another and with the theoretical estimates derived by supersonic area rule. The different experimental values are shown to be self-consistent and to lie up to 30% below the theoretical estimates.

---

* This work was performed by Engineering Sciences Data Unit Ltd under MOD(PE) contract for Aerodynamics Department, RAE Farnborough.

** Consultant to Engineering Sciences Data Unit Ltd.

*** Engineering Sciences Data Unit Ltd.

**** Replaces RAE Technical Report 76072 - ARC 37297

CONTENTS

		Page
1	INTRODUCTION	3
2	DELTA WING WITH BICONVEX CENTRE SECTION	3
	2.1 Description of the model and the tests	3
	2.2 Derivation of the pressure drag from the measured pressure distribution	5
	2.3 Comparison of the experimental values of the zero-lift wave drag with those from the supersonic area rule	10
	2.4 Analysis of the balance measurements	12
3	DELTA WINGS WITH LORD V AREA DISTRIBUTION	13
	3.1 Wings with different volume	13
	3.2 Wings of different aspect ratio	17
4	DELTA WINGS WITH DIFFERENT TYPES OF CROSS SECTION	20
5	WING WITH GOTHIC PLANFORM	21
6	CONCLUSIONS	22
Appendix A	The zero-lift wave drag according to linear theory	25
Appendix B	Evaluation of the constant k in equation (A-15)	35
Appendix C	Derivation of the zero-lift drag from balance measurements	38
Appendix D	Experimental results for the lift-dependent drag factor	40
Appendix E	Estimate of the skin-friction drag	41
Table 1	Geometry of delta and gothic wings tested in the 8ft × 8ft tunnel	45
Symbols		46
References		47
Illustrations		Figures 1-29
Detachable Abstract Cards		-

1 INTRODUCTION

In 1957-59 a number of slender wings of fairly simple shape were tested at supersonic speeds in the 8ft × 8ft tunnel at RAE Bedford by A.O. Ormerod. The results contributed to the evolution of aerodynamic shapes suitable for application to supersonic transport aircraft, but the work was not reported in detail at the time. The opportunity has now been taken to examine the results more clearly, in particular those for a series of delta wings with rhombic cross sections.

Obvious difficulties arise in the analysis of measurements made more than 15 years ago, partly because certain details were not thought significant at the time and now cannot be recalled, partly because the techniques then used now appear somewhat unrefined. Nonetheless, some analysis still appears to be worthwhile.

This Report is primarily concerned with the zero-lift wave drag. For one wing, which had a biconvex centre section, detailed measurements of surface pressure were made in addition to the usual three-component balance measurements. The analysis of the results for this particular wing is dealt with in section 2.

For two series of delta wings with the so-called Lord V area distribution (see Ref.1) and varying aspect ratio and volume, balance measurements and some pressure distributions are available. The analysis of these results is discussed in section 3.

Some further tests were made on delta wings with different types of cross sections and on a wing of a different planform. The analysis of these results is discussed in sections 4 and 5.

2 DELTA WING WITH BICONVEX CENTRE SECTION

2.1 Description of the model and the tests

The model, model 229 of Table 1, was a delta wing of length $c_0 = 60$in (= 1.524m) and semispan $s = 20$in (= 0.508m), so the aspect ratio was 4/3. The centre section was given by

$$\frac{z}{c_0} = \pm 0.18 \frac{x}{c_0}\left(1 - \frac{x}{c_0}\right)$$

where axes are chosen with x measured along the centre line from the apex,

y to starboard and z upwards. This corresponds to a parabolic biconvex centre section with a thickness-to-chord ratio of 9%. The basic cross sections of the wing were diamond-shaped, but to provide sufficient strength the wing was thickened near the tips. Thickness was added outboard of the straight lines joining the points on the leading edges at $x_{LE}/c_0 = 0.9$ to the points on the trailing edge where $|y_{TE}/s| = 0.65$, as shown in Fig.1. Outboard of each of these lines the wing shape was conical, with vertex at the tip.

For the pressure measurements the wing was strut-mounted from below, in such a way that the upper surface was free of interference at the Mach numbers of the tests. For the balance measurements the model was supported by a sting with a symmetrical shroud in the form of a circular cylinder of diameter 2.5in (63.5mm) running forward from the base until it merged into the wing thickness.

Along the leading edge on each surface was a transition strip of width 0.25in (6.4mm) consisting of 100 grade carborundum grit embedded in aluminium paint. The tests analysed in this Report were made at a Reynolds number based on the wing chord, c_0, of $R_{c_0} = 10^7$ at Mach numbers up to 2.4 and of $R_{c_0} = 7.5 \times 10^6$ at Mach numbers of 2.6 and 2.8. Experience suggests that for $R_{c_0} = 10^7$ the strips would cause boundary-layer transition for free-stream Mach numbers up to 2.0, but that for higher Mach numbers they might become progressively less effective.

The surface pressure was measured at holes of diameter 0.8mm drilled normal to the surface and connected to weighbeam capsule manometers. The positions of the holes are shown in Fig.1.

The balance measurements were reduced to coefficient form at the time of the tests. The usual corrections were applied; in particular, the axial force coefficient was adjusted to correspond to free-stream static pressure within the sting shroud.

When the coefficients of drag and normal force were plotted against the angle of incidence, α, it was found that the curves were not exactly symmetrical or antisymmetrical about $\alpha = 0$. This error, which occurred at all Mach numbers, but with somewhat varying magnitude, may be attributed to flow misalignment, to instrument errors or to asymmetry of the model. Since the error was less than 0.1°, it seems justifiable to ignore its effect on the pressure distribution and the normal pressure drag at zero nominal incidence. With respect to the results from the balance tests, an attempt is made to take account of the asymmetry of the $C_D(C_L)$ curves, as described in Appendix C.

It has been estimated (see Appendix C) that the accuracy of the measured drag coefficients is about ±0.0002 at Mach numbers from 1.4 to 2.4 and ±0.0003 at Mach numbers of 2.6 and 2.8.

2.2 Derivation of the pressure drag from the measured pressure distribution

Though the number of pressure holes was fairly large (53 on the upper surface of the wing) for a model of such simple geometry, it is still difficult to specify the accuracy with which the overall forces can be determined by integrating the pressure distribution. This is a result of lack of information, in particular, close to the leading edge. Further, the pressure coefficients, $c_p(x,y)$, measured at a spanwise station y , when plotted against the chordwise coordinate x , do not all lie on smooth curves; this could be due to defects in the pressure holes. To derive a plausible pressure distribution for the whole wing, it is necessary to draw smooth curves through the measured values of c_p and to extrapolate the curves to the leading and trailing edges.

The available theoretical results are based on thin-wing theory or on slender-body theory. Thin-wing theory produces perturbation velocities which tend to infinity at the leading edge; therefore thin-wing theory cannot be used as a guide to extrapolating the experimental values of the pressure coefficient towards the leading edge. For the lowest Mach number of the tests, $M = 1.6$, the slenderness parameter $\beta s/c_0$ is larger than 0.4; it was therefore not considered to be worth the effort to compute the pressure distribution by slender-body theory. (The angle, δ , at which the upper and lower surfaces meet along the leading edge of the delta wing discussed here is given by

$$\delta = \tan^{-1}(0.54(1 - x/c_0)) \quad .$$

This rises to 30° near the apex. Britton[2] has measured pressure distributions on a cone with rhombic cross-sections for which $\delta = 30^\circ$ and found that, even for $\beta s/c_0$ as small as 0.2, the experimental values of c_p did not agree at all closely with those calculated by slender-body theory.)

An approximate pressure distribution has therefore been derived by graphical means. For each free-stream Mach number the values of $c_p(x,y)$ measured for constant values of y have been plotted as functions of x . c_p was also plotted against y for constant values of x ; on this diagram curves have been drawn through the values of $c_p(x,y)$ for points (x,y) which have the same distance from the leading edge, that is, $y/c_0 = (x/3c_0) - \text{constant}$. By transferring information from one plot to another, a plausible smooth pressure

distribution for the whole wing up to the leading and trailing edges was derived. From these plots values of c_p were tabulated for the spanwise stations $y/s = 0,\ 0.05,\ 0.225,\ 0.4,\ 0.55,\ 0.75$ (except for $y = 0$, these are the spanwise stations at which c_p values were measured). This procedure has been carried out for the free-stream Mach numbers 1.6, 2.0, 2.4, 2.8.

Using the smoothed values of $c_p(x,y)$, one can derive values for the sectional drag coefficient $C_D(y)$ by plotting $c_p(x;y)$ against the local wing ordinate $z(x,y)$:

$$C_D(y) = \frac{D(y)}{\frac{1}{2}\rho_0 V_0^2 c(y)}$$

$$= \frac{2}{c(y)/c_0} \int_{y/s}^{1} c_p(x;y) \frac{\partial z(x;y)}{\partial x} \, d\left(\frac{x}{c_0}\right)$$

$$= \frac{2}{1 - y/s} \int c_p(x;y) \, d\left(\frac{z(x;y)}{c_0}\right) ,$$

where $c(y)$ is the local chord of the wing.

The coefficient of the total normal pressure drag, D_w, can be determined from the relation

$$C_{D_{0w}} = \frac{D_w}{\frac{1}{2}\rho_0 V_0^2 s c_0}$$

$$= \int_0^1 2C_D(y) \frac{c(y)}{c_0} \, d\left(\frac{y}{s}\right)$$

$$= 2 \int_0^1 \left\{ 2 \int_{y/s}^{1} c_p \frac{\partial z(x,y)}{\partial x} \, d\left(\frac{x}{c_0}\right) \right\} d\left(\frac{y}{s}\right) . \qquad (1)$$

The following results have been obtained:

M	$C_{D_{0w}}$	K_0
1.6	0.01012	0.828
2.0	0.00821	0.672
2.4	0.00738	0.604
2.8	0.00647	0.529

It is helpful to compare the wave drag of a configuration with that of the Sears-Haack body of the same length and the same volume. (This is the body of revolution with zero nose and base areas which, according to slender-body theory, has the lowest wave drag for a prescribed length and volume.) The theoretical value for the wave drag of a Sears-Haack body of length c_0 is

$$\frac{D_{w\ S-H}}{\frac{1}{2}\rho_0 V_0^2 c_0^2} = \frac{128}{\pi}\left(\frac{\text{vol}}{c_0^3}\right)^2 .$$

The zero-lift wave-drag factor, K_0, is defined as the ratio of the wave drag of the given configuration to that of the Sears-Haack body of the same length and volume:

$$K_0 = \frac{D_w}{D_{w\ S-H}} = \frac{\pi}{128}\frac{D_w}{\frac{1}{2}\rho_0 V_0^2 c_0^2}\frac{1}{\left[\text{vol}/c_0^3\right]^2} . \tag{2}$$

The delta wing discussed here had the non-dimensional volume: $\text{vol}/c_0^3 = 0.01$. (The thickening of the wing tips increases the volume by a negligibly small amount, namely 0.0004 times the volume of the basic wing.) The quoted K_0 values are therefore derived from the relation

$$K_0 = \frac{\pi}{128} C_{D_{0w}} \frac{sc_0}{c_0^2}\frac{1}{0.01^2}$$

$$= \frac{\pi}{3 \times 1.28} 100 C_{D_{0w}} . \tag{3}$$

The procedure by which we have determined the wave drag from the measured pressure coefficients produces values which may be in error by 1-2%. This

uncertainty is mainly a consequence of the fact that it was necessary to smooth the pressure distributions and in particular that it was necessary to extrapolate the pressure coefficients to the leading edge (where the slope $\partial z/\partial x$ is fairly large). The estimate for the possible error was derived by plotting and interpolating a second time the values of $c_p(x,y)$ and determining $C_D(y)$ and $C_{D_{0w}}$. We may also mention that in the past others have integrated some of the pressure distributions; they have obtained values for the pressure drag which differ from those quoted above by not more than 3%.

One may expect that the graphical procedure for deriving the drag from a known pressure distribution introduces an error of less than 1%. To confirm this estimate, the procedure has been checked in the following way. The theoretical pressure distribution given by linear theory has been computed for $M = 2$. For the wing without tip modification an analytic expression for c_{p_ℓ} is known, see e.g. Ref.3. Using the computed pressure distribution at the same spanwise stations as for the experimental pressure distribution, the theoretical wave drag has been determined by the same graphical procedure as was used for the experimental value. To overcome the graphical difficulty introduced by the infinite theoretical pressure coefficient at the leading edge, the term

$$c_{p_s} = \frac{0.18\sqrt{6}}{3\pi} (1 - 3y/c_0) \log \frac{1 - 3y/c_0}{1 - 3y/x}$$

was subtracted from the linear theory value, c_{p_ℓ}, and the integral

$$\int_{y/s}^{1} \left[c_{p_\ell}(x;y) - c_{p_s}(x;y) \right] \frac{\partial z(x;y)}{\partial x} \, d\left(\frac{x}{c_0}\right)$$

was determined graphically. In this way we obtained a value for the wave drag factor, according to linear theory, $K_{0_\ell} = 0.792$.

The wave drag, according to linear theory, can also be derived by the supersonic area rule. By the numerical method described in Appendix A, we have obtained, for $M = 2$, the value $K_{0_\ell} = 0.789$ which is about 0.5% less than the value above. The area rule involves the evaluation of a triple integral, see equation (A-3), which cannot be performed analytically. To derive values for the inner double integral, equation (A-13), we have applied Eminton's

technique[4], using values of the oblique cross-sectional area at 40 chordwise points. Eminton's method gives for the double integral the minimum value for the family of possible area distributions which have the prescribed values at the 40 points. (We note that if the triple integral were evaluated exactly and the pressure distribution were integrated exactly, the resulting drag values would agree exactly; there is no higher order difference.) The difference of about 0.5% between the two values for K_{0_ℓ} may therefore overestimate the error involved in the graphical procedure used for deriving the wave drag from a known pressure distribution.

We have mentioned that the wing has been thickened near the tips. For $\beta = \sqrt{M^2 - 1} > 1.2$ (i.e. $M > 1.56$), according to linear theory the tip modification can alter the pressure distribution on the wing only in the region where the tip is modified. The pressure coefficient has been measured at only one point in the area of the tip modification. We have computed by supersonic area rule the wave drag of the wing with and without tip modification; it is found that, for $1.6 \leqslant M \leqslant 2.8$, the tip modification increases the drag by less than 0.25%, $\left(\Delta D_{w_\ell \text{ mod}} \Big/ D_{w_\ell} < 0.0025\right)$. We may therefore assume that the lack of details of the pressure distribution over the modified tips is not important. (The tip modification has only a very small effect on the wave drag because the outboard part of the wing makes only a small contribution; the spanwise integral of the sectional drag over the part of the wing outboard of the stations $|y/s| = 0.65$ contributes less than 3% to the wave drag of the wing.)

The speed in the empty tunnel is not precisely uniform. This speed variation affects the measured pressure distribution and might therefore entail a correction to the normal pressure drag. The original analysis of the data was based on calibrations of the flow in the tunnel made in 1957-58. More comprehensive calibrations were undertaken in 1961 and the results from these calibrations have been used in re-assessing the analysis, though it should be noted that some changes had been made between the two calibrations to the working-section flexible-wall system. In the later calibration the Mach number and flow direction were measured in horizontal and vertical planes through the tunnel axis. The results of the measurements in the horizontal plane were very nearly independent of spanwise position, and so we have taken the correction to the static pressure appropriate to the axis of the tunnel to apply over the span of the wing. By integrating this correction to c_p over the wing, see equation (1), we obtain a correction to $C_{D_{0w}}$. For the Mach numbers $M = 1.6$, 2.0, 2.4 and 2.8, the

correction is not larger than about ±0.0001. Since the correction is small (and because we do not have the information relevant to the period of the tests), we ignore the term in the following analysis.

One would also like to know how much the boundary layer affects the pressure distribution and the normal pressure drag at zero lift. To obtain an estimate of this effect, J.H.B. Smith (RAE unpublished) has determined the displacement thickness, using the method suggested by Cooke[5]. By linear theory, he computed the pressure distribution due to the boundary layer displacement thickness for $M = 2$ and the spanwise stations $y/s = 0.05, 0.225, 0.4$. The calculations have been done for zero pressure gradient, with and without allowance for streamline convergence on the centre line. Integration of the pressure distribution obtained without allowance for streamline convergence produces an increase of the pressure drag coefficient of about 0.00006, i.e. less than 1%. The pressure distribution calculated with allowance for the streamline convergence produces at the station $y/s = 0.05$ a reduction in the local pressure drag, $C_D(y)$, and at the stations $y/s = 0.225$ and 0.4 an increase. These values suggest that the boundary layer changes the pressure drag of the whole wing by a negligible amount. Consequently, in what follows we shall neglect the form drag, i.e. the pressure drag due to viscosity, and regard the drag as the sum of the inviscid pressure drag and the friction drag.

2.3 Comparison of the experimental values of the zero-lift wave drag with those from the supersonic area rule

The theoretical estimates for the zero-lift wave drag available at present are derived by the supersonic area rule, which is based on linear thin-wing theory, or by slender-body theory. In Appendix A (equation (A-3)) we quote a formula from which the drag can be derived and we discuss the practical procedure for the computation.

The zero-lift wave-drag factor derived from the supersonic area rule, K_{0_ℓ} , is plotted in Fig.2. We note that the tip modification increases the values of K_{0_ℓ} by only a small amount: at $M = 1.6$, $\Delta K_{0_{\ell\ \mathrm{mod}}} = 0.002$; at $M = 2.0$, $\Delta K_{0_{\ell\ \mathrm{mod}}} = 0.0017$; at $M = 2.6$, $\Delta K_{0_{\ell\ \mathrm{mod}}} = 0.0013$; so that the curve drawn applies to the basic wing and to the wing with modified tips.

We have also plotted the values of K_{0_s} , the zero-lift wave-drag factor derived from slender-body theory, equation (A-18). This equation is derived from the linear theory expression, equation (A-17), by neglecting the terms of

order $\beta s \log \beta s$ and the terms of order βs . For $M = 1.6$, $\beta s = 0.416$ and $\beta s \log \beta s = -0.365$; it is therefore not surprising that the result from slender-body theory (which is the same as that from slender thin-wing theory) differs appreciably from that from the non-slender theory.

We have plotted the values of slender theory both for the basic wing and for the wing with modified tips to demonstrate that results from slender theory can be quite useless. The reason for the failure of the slender theory is the behaviour of the area distribution $S(x)$, obtained by cuts $x = \text{constant}$, near the trailing edge. For the wing with modified tips, the second derivative $S''(x)$ tends logarithmically to infinity at the trailing edge.

Fig.2 shows that the supersonic area rule gives larger values for the wave drag than the experiment. The error $\left(K_{0_\ell} - K_{0\ exp}\right) \Big/ K_{0_\ell}$ increases from about 0.1 at $M = 1.6$ to about 0.2 at $M = 2.8$.

To show the origin of the difference between the experimental values for the zero-lift wave drag and the values from linear theory, we have plotted in Fig.3, for the station $y/s = 0.05$ and $M = 2$, the pressure coefficient c_p against the z-ordinate of the wing. We have plotted the smoothed experimental values and the theoretical values c_{p_ℓ} . (As mentioned above, for $M = 2$, the tip modification does not affect the pressure distribution at $y/s = 0.05$.) To demonstrate that the discrepancies at this station are typical, we quote that, for this station,

$$\int_{y/s}^{1} c_{p_\ell}(x, y/s = 0.05) \frac{\partial z}{\partial x} \, d\left(\frac{x}{c_0}\right) = 0.00711$$

and

$$\int_{y/s}^{1} c_{p\ exp}(x, y/s = 0.05) \frac{\partial z}{\partial x} \, d\left(\frac{x}{c_0}\right) = 0.00595$$

$$= 0.837 \times 0.00711$$

while, for the whole wing

$$C_{D_{0w\ exp}} \Big/ C_{D_{0w\ell}} = 0.847 \quad .$$

The figure shows that for the wing considered the difference between the experimental and the theoretical c_p-values is larger over the rear of the wing (given by the upper branches of the curves) than over the front, except very close to the leading edge. The discrepancy is certainly not confined to the immediate neighbourhood of the leading edge, where the theory predicts a singularity.

2.4 Analysis of the balance measurements

It has already been stated that, for a wing of the same shape as the pressure plotting model, lift, drag and pitching moment were measured by a strain gauge balance on a model supported by a sting enclosed in a cylindrical shroud.

As mentioned in section 2.1, the plots of the measured values of C_D as functions of C_L are not strictly symmetrical about the line $C_L = 0$. We describe in Appendix C how we have derived from the measured C_D and C_L values an approximation to the zero-lift drag of a symmetrical wing in uniform flow. Values of C_{D_0} are plotted in Fig.4. The uncertainty is indicated in the figure.

To determine how much of the measured drag is wave drag we need an estimate for the drag produced by skin friction, C_{D_F}. In Appendix E, we describe how we obtain an estimate of C_{D_F}. This estimate is also plotted in Fig.4. For $M \leqslant 2.4$ the tests were done at a Reynolds number based on the wing centre-line chord, $R_{c_0} = 10^7$; for $M > 2.4$ the Reynolds number was reduced to $R_{c_0} = 0.75 \times 10^7$. This change in Reynolds number is the reason for the discontinuity in the $C_{D_F}(M)$ curve. We have included in the figure the drag values for the flat plate delta wing. The difference between this value and C_{D_F} takes account of the fact that the thick wing has a larger wetted area than the thin wing and it includes an estimate for the drag increase produced by the transition strips. Fully turbulent flow has been assumed for all Mach numbers.

We have added to C_{D_F} the theoretical value of the wave drag, $C_{D_{0w}}$, for the wing with the sting shroud present. Both the value calculated by the supersonic area rule and the value from slender-body theory have been used. For the value from slender-body theory we have ignored the tip modification for the reason discussed in section 2.3.

Fig.4 shows that the sum of C_{D_F} and $C_{D_{0w\ell}}$, from linear theory, is larger than the experimental drag coefficient.

The difference between the measured C_{D_0} and C_{D_F} gives the experimental value of the zero-lift wave drag for the configuration with the sting shroud. In practice, we are interested in the wave drag of the wing without sting. As an estimate of the sting effect, $\Delta C_{D_{0w}}$, we take the difference between the theoretical values of the wave drag for the wing alone and for the wing with the sting shroud, computed by the area rule. $\Delta C_{D_{0w}}$ is positive, which means that the presence of the sting shroud lowers the wave drag. Values of $C_{D_0} - C_{D_F} + \Delta C_{D_{0w}}$ are plotted in Fig.5, together with the values of $C_{D_{0w}}$ obtained from the measured pressure distributions.

Fig.5 shows surprisingly close agreement between the two sets of values for $C_{D_{0w}}$ which have been derived from the measurements. This agreement may be somewhat accidental; we may have used slightly too large values for both C_{D_F} and $\Delta C_{D_{0w}}$. To allow some assessment of the magnitude of the possible errors, we have plotted in the figure the sting correction $\Delta C_{D_{0w}}$ and the difference between the estimated values of C_{D_F} and the friction drag for a thin flat delta wing. This difference takes account only of the difference in wetted area between the thick and the thin wing (and of the drag increase from the transition strips) and not of any effects which pressure gradients and streamline convergence may have on the local skin friction. The agreement between the two sets of values for $C_{D_{0w}}$ supports this method of assessing the skin friction. The fact that the agreement between the value of the wave drag obtained from the integrated pressure distribution and the value derived from the balance test is as close at $M = 2.8$ as at $M = 2.0$ suggests that the analysis described in Appendix C has eliminated the effects of any laminar flow occurring at the higher Mach number. In Fig.5, we have also plotted the theoretical zero-lift wave drag for the wing without sting shroud. As already shown in Fig.2, the supersonic area rule overestimates the wave drag by more than 10%.

3 DELTA WINGS WITH LORD V AREA DISTRIBUTION

3.1 Wings with different volume

Three further delta wings of aspect ratio 4/3 and with rhombic cross sections have been tested. Their cross sectional area distribution is the so-called Lord V distribution (see Ref.1). The centre section of the wing is defined by the equation

$$\frac{z(x,0)}{c_0} = \frac{vol}{c_0^3}\, 10.5\, \frac{x}{c_0}\left(1 - \frac{x}{c_0}\right)\left[4 - 6\,\frac{x}{c_0} + 4\left(\frac{x}{c_0}\right)^2 - \left(\frac{x}{c_0}\right)^3\right] \quad .$$

The wings had different volumes: $vol/c_0^3 = 0.01$; 0.0075 and 0.005625. The tips were thickened in a conical fashion, as on model 229, but because the basic wings were thinner near the tips than the wing with biconvex centre section, the tip modification extended over a larger part of the plan area. Details for the three models discussed here, models 233, 234, 240, are quoted in Table 1. For the balance measurements the wings were supported by the same sting as was used with model 229; the same kind of transition strips was used with all the models.

The zero-lift drag for the three wings has been derived from the tabulated results of the balance tests in the manner described in Appendix C. The values are plotted in Figs.6, 7 and 8 together with the estimated values of the skin-friction drag C_{D_F} derived in Appendix E. The sum of C_{D_F} and the theoretical value of the wave drag (calculated by the supersonic area rule for the wings with sting shroud and modified tips) is also plotted in the figures.

We note again that the experimental values of the zero-lift drag are smaller than the estimated values.

Since we are mainly interested in the values of the wave drag for the wings without sting shroud, we have again derived the values of $C_{D_0} - C_{D_F} + \Delta C_{D_{0w\ell}}$, where the values of the sting correction are obtained by the supersonic area rule. We may mention that for model 234 pressure measurements have been made to determine the increase in wave drag due to removing the sting shroud. At $M = 2$, the value of the increase in wave drag derived from the measurements is $\Delta C_{D_{0w}} = 0.00041$ whilst the area rule gives $\Delta C_{D_{0w\ell}} = 0.00043$.

The extent of the tip modification was somewhat different on the three models. To compare the drag for wings of the same geometry, we have subtracted from $C_{D_0} - C_{D_F} + \Delta C_{D_{0w\ sting}}$ the theoretical value, $\Delta C_{D_{0w\ mod}}$, for the change in wave drag produced by the tip modification. $\Delta C_{D_{0w\ mod}}$, though larger than for model 229, is a small term; at $M = 2.0$

Model	$\Delta D_{w\ell\ mod}/D_{w\ell}$
233	0.005
234	0.013
240	0.014

In Fig.9, we have plotted the experimental value of the zero-lift drag factor K_0 (derived from $C_{D_0} - C_{D_F} + \Delta C_{D_{0w\ sting}} - \Delta C_{D_{0w\ mod}}$ and equation (2)) for the three wings of different volume.

Some pressure distributions have been measured on the three delta wings at $M = 1.6$ and at $M = 2.0$. By integrating the pressure distribution on the wing with $\mathrm{vol}/c_0^3 = 0.01$ we obtain at $M = 1.6$: $C_{D_{0w}} = 0.00825$ and at $M = 2.0$: $C_{D_{0w}} = 0.0076$. These values are close to the results obtained from the balance tests; at $M = 1.6$: $C_{D_0} - C_{D_F} + \Delta C_{D_{0w\ \mathrm{sting}}} = (1.311 - 0.576 + 0.075) \times 10^{-2} = 0.0081$; at $M = 2.0$: $C_{D_0} - C_{D_F} + \Delta C_{D_{0w\ \mathrm{sting}}} = (1.222 - 0.529 + 0.057) \times 10^{-2} = 0.0075$.

The determination of $C_{D_{0w}}$ from the pressure distributions measured on the wing with $\mathrm{vol}/c_0^3 = 0.0075$ is rather uncertain because the number of points near the leading edge at which the pressure has been measured is small. Moreover, due to the relatively large chordwise slope near the leading edge of the wings with Lord V area distribution, the part of the wing near the leading edge makes a considerable contribution to the pressure drag. We therefore refrain from quoting the drag obtained from the pressure distribution on this wing.

For the thinnest of the three wings, with $\mathrm{vol}/c_0^3 = 0.005625$, we obtain at $M = 2.0$: from the pressure distribution $C_{D_{0w}} = 0.00253$ and from the balance test: $C_{D_0} - \Delta C_{D_F} + \Delta C_{D_{0w\ \mathrm{sting}}} = (0.731 - 0.515 + 0.032) \times 10^{-2} = 0.00248$.

We have again subtracted the estimated drag increase due to the tip modification and have determined the experimental values of the zero-lift drag factor K_0. The values are plotted in Fig.9 and are quoted for $M = 2.0$ in the following table:

$\frac{\mathrm{vol}}{c_0^3}$	K_0 from measured pressures	K_0 from balance test	ΔK_0 due to sting shroud	ΔK_0 due to tip modification	ΔK_0 corresponding to excess friction drag	ΔK_0 corresponding to ± 0.0002 in C_D
0.01	0.618	0.610	0.047	-0.004	-0.030	±0.016
0.0075		0.622	0.063	-0.009	-0.041	±0.029
0.00563	0.643	0.632	0.083	-0.009	-0.059	±0.052

The K_0-values from the pressure distributions are again surprisingly close to those from the balance tests. To demonstrate how far this agreement may be fortuitous, we have included in the table the contributions to K_0 which correspond to the sting correction, the contribution from the tip modification, the equivalent contribution which corresponds to the difference between the estimate for the friction drag of the wing with transition strips and the friction drag of the smooth flat-plate delta wing with fully turbulent flow, and the uncertainty

in K_0 which corresponds to the possible error in the balance measurements. Finally, the drag values obtained from the pressure distribution are themselves uncertain by about ±2%.

The theoretical value at $M = 2.0$ is $K_{0_\ell} = 0.736$. From the numbers in the table one might conclude that the percentage error in the prediction of the wave drag by linear theory decreases with decreasing wing thickness. However when we consider all the experimental K_0-values plotted in Fig.9 for the various Mach numbers, no such conclusion emerges. We have drawn a mean curve through the K_0-values for the wing with the largest volume; these K_0-values do not depart much from the curve. For the thinnest wing, some K_0-values lie below the curve drawn and some lie above, whilst for the intermediate thickness more values lie above than below the curve. We have marked in the figure the uncertainty in the K_0-values which arises from the uncertainty in the measured drag coefficients. In view of the size of this uncertainty, we cannot claim that the area rule produces a more accurate estimate of the wave drag for thinner wings, for which the small disturbance theory would be expected to be more accurate.

To examine further how the validity of linear theory for wings of similar geometry varies with the thickness of the wing, we have examined some of the measured pressure distributions. In Fig.10 we have plotted the value of $\frac{0.01}{\text{vol}/c_0^3} c_p(x,y)$, for $y = 0.05s$ and $M = 2$, from the measurements on the three wings and from linear theory. The figure shows that for model 234, with $\text{vol}/c_0^3 = 0.0075$, the values lie between those for the thicker wing, model 233 with $\text{vol}/c_0^3 = 0.01$, and c_{p_ℓ} . For the thinnest wing, model 240 with $\text{vol}/c_0^3 = 0.00563$, the values over the forward part lie between those for model 234 and c_{p_ℓ} , but this is not so at the rear of the wing. A similar pattern is found for the spanwise stations further outboard and also for the pressure distributions at $M = 1.6$. Apart from the values at the rear of model 240, Fig.10 (and the similar behaviour of c_p for other values of y and also for $M = 1.6$) would suggest that the percentage error in the pressure distribution obtained by linear theory decreases with decreasing thickness. For a two-dimensional aerofoil the value of $\left|c_p(x) - c_{p_\ell}\right| / (t/c)$ decreases nearly linearly with decreasing thickness-to-chord ratio t/c . From the pressure distributions measured on the three delta wings we cannot discover how the difference $\left|c_p - c_{p_\ell}\right| / \left(\text{vol}/c_0^3\right)$ decreases with decreasing volume; this means that we are not yet able to say how the value of $K_{0_\ell} - K_0$ varies with volume.

We note that even for the thinnest wing, model 240 (which has the mean thickness t^* = volume/(planform area) = $0.01688c_0$) , the assumption of the wing being thin is not satisfied everywhere. Near the apex the wing is similar to a cone of rhombic cross section with the edge angle $2\delta = 2 \times 35.3^\circ$. The edge angle 2δ of sections $x = \text{const}$ is given by

$$\tan \delta = \left|\frac{\partial z(x,y)}{\partial y}\right| = 0.708 \left(1 - \frac{x}{c_0}\right)\left[1 - 1.5 \frac{x}{c_0} + \left(\frac{x}{c_0}\right)^2 - 0.25 \left(\frac{x}{c_0}\right)^3\right] \quad .$$

To improve the accuracy of the pressure distribution derived by linear theory, Cooke[6] has developed a 'not-so-thin' theory. However this theory does not allow the evaluation of the pressure drag, because the singular behaviour of the velocity near the leading edge is not known.

We may note that the measured c_p values plotted in Fig.10 differ from those plotted in Fig.7 of Ref.6 by 0.008. The values used in Ref.6, as those used here, contain a correction for the static pressure variation in the empty tunnel. We have made a further correction in that we have taken some account of possible effects of humidity on the static pressure, of the viscous effects on the pressure indicated by a static hole and of the effect of the boundary-layer displacement thickness. At $M = 2.0$ and $R = 2 \times 10^6$ per foot, the increase in static pressure due to water vapour condensation is up to $\Delta c_p = 0.0054$; a mean value for the static-hole viscous error is $\Delta c_p = 0.0008$; a mean value for the change in pressure produced by the displacement thickness is $\Delta c_p = 0.002$ (this value has been taken from the unpublished work by Smith, referred to in section 2.2); we have therefore subtracted 0.008 from the c_p-values used previously[6]. This correction has of course no effect on the pressure drag. To demonstrate how such a small correction can alter the comparison we have been making we have plotted the uncorrected values in Fig.11. The differences between Figs.10 and 11 illustrate that a high degree of experimental accuracy is required to produce meaningful comparisons.

The fact that the K_{0s} values derived by slender-body theory are independent of the volume is not relevant since we are interested in a range of Mach numbers for which the assumptions of slender theory do not hold.

3.2 Wings of different aspect ratio

Balance measurements were also made on a series of delta wings of different aspect ratios: A = 16/9, 4/3, 1.0, 2/3 . The wings had rhombic cross sections

and the same section along the centre line, namely the one of model 234, discussed in section 3.1. Details of the tip modification are given in Table 1.

Values of C_{D_0} have again been derived in the way discussed in Appendix C. The results are plotted in Fig.7 and Figs.12-14. We have again indicated the uncertainty in the measured values. It is assumed that the uncertainty in the measured drag force is the same for all the tests. Consequently the uncertainty in the drag coefficient is twice as large for the wing of aspect ratio 2/3 as that for the wings of aspect ratio 4/3, because all the models had the same centre-line chord. We have also plotted the estimated skin-friction drag C_{D_F}, and the sum of C_{D_F} and the estimate of the wave drag obtained by the area rule for the combination of the modified wing and the sting.

For the wing of aspect ratio 16/9, model 237, the leading edge becomes sonic at $M = 2.463$. For the reason discussed in Appendix A, we have computed the wave drag of delta wings only for subsonic leading edges; we have calculated the drag for $\beta s \leqslant 0.9$.

From the values of C_{D_0} we have again derived values of $C_{D_{0w}}$ (and K_0) by subtracting the estimated values of C_{D_F}, by adding the sting-shroud correction as given by the area rule, and by subtracting the theoretical value for the change in wave drag produced by the tip modification. The wave drag factor from linear theory depends only on the product βs and not on β and s separately. We have therefore plotted in Fig.15 the experimental values of K_0 against βs. For aspect ratio 4/3, we have added the mean curve from Fig.9 and have plotted the values for model 233, since they show less scatter than those for model 234. The figure shows that the experimental values of K_0, except those for the wing of aspect ratio 2/3, also depend solely on the product βs. For the wing of largest aspect ratio at $\beta s \geqslant 0.77$, i.e. $M \geqslant 2$, the values of $K_0(\beta s)$ are slightly lower than those of the mean curve. One may argue that this indicates that the flow was not fully turbulent. For this wing, the chordwise extent of the roughness band is smaller than on the other models; it is therefore possible that transition to fully turbulent flow was not achieved at the end of the transition strips. If this were so, then the values of C_{D_F} we have subtracted would be too large and the values of K_0 obtained would be too small. (We note that a 10% reduction in C_{D_F} increases K_0 by 0.05.)

Fig.15 shows that the values of $K_0(\beta s)$ for the wing of smallest aspect ratio are lower, by about 0.2, than those from the mean curve. To examine

whether this difference can be explained, we consider in the remainder of this section the various terms which contribute to the values of K_0 derived from the measurements.

For $M = 2$, we have listed in the following table the numerical values of the various contributions to the 'experimental' value for the zero-lift wave-drag factor K_0. The magnitude of the various terms is appreciably larger for the wing with aspect ratio 2/3 than for the other wings; this implies a larger uncertainty in the 'experimental' values of K_0. We note that, for the wings of smallest aspect ratio, a change in K_0 of 0.2 arises from a change in $C_{D_{0w}}$ of only 0.0007.

The largest contribution is produced by the skin-friction drag. The table shows that, for the wing of smallest aspect ratio, a reduction of the friction drag of the flat plate by 10% is equivalent to an increase in K_0 of 0.14. We have based the estimate of the skin-friction drag on the local friction coefficient of a flat delta wing, which implies that we have ignored the effect of pressure gradients and streamline divergence and convergence on the skin friction. Smith, Gaudet, Winter[7] have measured the local skin-friction on model 233 (aspect ratio = 4/3, $\text{vol}/c_0^3 = 0.01$) using the razor-blade technique. We cannot make full use of their measured values because the tests were done with free transition, so that the flow was laminar in some regions. However, Fig.14a of Ref.7 suggests that near the centre line of the wing the local skin friction over the rear of the wing is appreciably smaller than on a flat plate. The authors attribute this to the fact that the streamlines converge over the rear portion of the wing; this would tend to increase the boundary layer thickness and decrease the friction drag.

Contribution of various terms to the 'experimental' value of the zero-lift wave drag factor K_0, for delta wings with Lord V area distribution at $M = 2.0$

Model	Aspect ratio	$\frac{\text{vol}}{c_0^3}$	$\frac{K_0}{100 \times C_{D_{0w}}}$	β_s	K_{0_ℓ}	'$K_{0\ \text{exp}}$'	ΔK_0 due to sting shroud	ΔK_0 due to tip modification	K_0 corresponding to flat plate skin friction	ΔK_0 corresponding to excess skin friction drag	ΔK_0 corresponding to uncertainty in C_D
237	16/9	0.01	1.091	0.770	0.734	0.516	0.039	-0.010	-0.537	-0.021	±0.016
234	4/3	0.0075	1.455	0.577	0.736	0.622	0.063	-0.009	-0.716	-0.041	±0.029
239	1.0	0.00563	1.94	0.433	0.766	0.581	0.101	-0.011	-0.954	-0.081	±0.052
242	2/3	0.00375	2.91	0.289	0.823	0.552	0.180	-0.010	-1.431	-0.215	±0.116

There is no reason to expect more laminar flow on the model of smallest aspect ratio because the chordwise extent of the roughness bands is largest.

The table shows that the contribution to K_0 which is related to the difference between the skin-friction drag on the thick wing with transition strips and the drag of the smooth flat-plate delta wing is fairly large for model 242. Sixty per cent of this term arises because the effective wetted area (see Appendix E) of the thick wing is about 10% larger than for the corresponding flat plate. The estimated drag increase caused by the roughness bands is $\Delta C_D = 0.0003$. There is of course some uncertainty about this estimate. For all models we have taken nearly the same increase in the friction drag, $\Delta D_F \ \frac{1}{2}\rho_0 V_0^2 c_0^2$. However, the uncertainty of the value for ΔD_F is more important for model 242 than for the other models since the ratio $\Delta K_0/\Delta D_F$ varies as $1\Big/\left(\text{vol}\Big/c_0^3\right)^2$ (for model 242 this ratio is seven times as large as for model 233).

The sting correction also matters more for model 242 than for the other models. The term has been derived by linear theory (for model 242 and $M = 2$, slender-body theory gives a value which is 5% larger). Values for the 'experimental' K_0 which are too low would have been obtained if linear theory underestimated the sting effect, but we cannot produce any argument for expecting a large underestimate.

Finally, we consider the effect of the assumption made about the accuracy of the balance measurements. The uncertainty in terms of the drag force, ΔD , is assumed to be the same for all models and so the uncertainty in the drag factor, K_0 , for model 242 is four times that for model 234. The uncertainties for $M = 2$ are shown in the table, and for the range of test Mach numbers in Fig.15.

As mentioned, the values of K_0 derived from the existing balance measurements with the wing of aspect ratio 2/3 are appreciably smaller than the values derived for the wings with larger aspect ratios. We have shown that the accuracy of the measurements and of the analysis is insufficient to conclude that a similar behaviour would be found if the zero-lift wave drag were measured more accurately.

4 DELTA WINGS WITH DIFFERENT TYPES OF CROSS SECTION

Balance measurements were made on two further delta wings, models 230 and 231 of Table 1. Both wings had a biconvex centre section, one wing had elliptic cross sections, the other had parabolic cross sections. The aspect ratio and

the volume of the two wings were the same as for model 229. In sections $x = \text{const}$, the three wings had therefore the same area: $S(x) = 0.12x^2(1 - x)$.

No tip modification was made on the wing with elliptic cross sections. On the wing with parabolic cross sections, the tip modification was smaller than on the wing with rhombic cross sections. We have seen above that the tip modification on model 229 increases the wave drag by a very small amount $(\Delta D_{w_{\ell\ \mathrm{mod}}}/D_{w_\ell} < 0.0025)$; in the following analysis we therefore ignore the tip modification of model 231.

Values of C_{D_0} have again been derived in the way discussed in Appendix C. The results are plotted in Figs.16 and 17 together with the estimated skin-friction drag, C_{D_F} , and the sum of C_{D_F} and the estimate of the wave drag, $C_{D_{0w}}$, obtained by the area rule for the combination of the wing and the sting.

From the values of C_{D_0} we have again derived values for the coefficient of the wave drag, $C_{D_{0w}}$, for the wings without sting shroud, by subtracting the estimated values of C_{D_F} and by adding the sting-shroud correction as given by the area rule. The values of $C_{D_{0w}}$ derived from the balance measurements for the three wings are plotted in Fig.18, together with the values from linear theory. For the wing with elliptic cross sections, we have plotted in Fig.18 the theoretical values given by Squire[8] in analytical form. (We note that we have compared some of the values with those obtained from the computer program and found good agreement.) Fig.18 shows that linear theory predicts at $M = 1.6$ for the wing with rhombic cross sections a wave drag which is about 9% larger than for the wing with elliptic cross sections; at $M = 2.8$ the drag predicted for the wing with rhombic cross sections is about 12% smaller than for the wing with elliptic cross sections. Fig.18 shows that the measured wave drag depends less on the shape of the cross section than linear theory predicts, both for βs small and for βs approaching 1. For $M = 2$ and 2.2 the measured variation is consistent with the predicted variation within the range of uncertainty.

5 WING WITH GOTHIC PLANFORM

At the time when the measurements were made on the delta wings, balance measurements were also made on one wing with a different planform, model 238. The wing had a so-called gothic planform, which is defined by

$$s(x) = \frac{1}{3}x(2 - x) \quad .$$

The wing had streamwise tips; its aspect ratio was 1.0. The centre section of the wing was given by the equation

$$z(x,0) = 0.105x(1 - x)(2 - 2x + x^2) \quad .$$

The wing had rhombic cross-sections, so that the area distribution of model 238 was

$$\begin{aligned} S(x) &= 2z(x,0)s(x) \\ &= 0.07x^2(1 - x)(4 - 6x + 4x^2 - x^3) \quad . \end{aligned}$$

This is the same Lord V area distribution as for model 233.

From the balance measurements we have derived values of C_{D_0} and have plotted these in Fig.19. We note that measurements were made only for $M \leqslant 2.4$.

Using these values of C_{D_0} we have again derived values of the zero-lift wave drag coefficient, $C_{D_{0w}}$, and of the zero-lift drag factor K_0. These values of K_0 are plotted in Fig.20 together with the values from linear theory. Since model 238 has the same chordwise area distribution $S(x)$ and cross-sectional shape as model 233, we have included in Fig.20 the values of K_0 for model 233, derived from the balance measurements and from linear theory. We see that linear theory predicts a lower wave drag for the gothic wing than for the delta wing (whilst slender-body theory predicts the same wave drag). The values obtained from the balance measurements confirm that the drag of the gothic wing is lower than that of the delta wing, though not to the extent predicted by the theory.

6 CONCLUSIONS

For a series of wings, values of the zero-lift wave drag have been derived by integrating measured pressure distributions and from the zero-lift drag coefficient obtained from balance measurements. The agreement of the values of the wave drag derived by the two sets of measurements gives some confidence in the estimates, used with the balance measurements, for the skin-friction drag and the sting correction.

The drag values obtained from the experimental results have been compared with those derived by linear theory. It was found that, for all the wings

tested, linear theory consistently predicts larger values for the zero-lift wave drag than those obtained from the experiments. The relative error is plotted in Fig.21. The figure indicates that the error increases with increasing βs . Apart from the flagged symbols, which relate to the wing of particularly low aspect ratio discussed in section 3.2, the errors lie within a well-defined band.

For delta wings with the same type of area distribution and cross section shape, it was found that the error does not depend on the volume, within the range examined: $0.0056 \leqslant \mathrm{vol}/c_0^3 \leqslant 0.01$. For a fixed value of βs , it was also found that the error does not vary systematically with the aspect ratio. On the other hand, the error does depend on the area distribution, as shown in Fig.22, on the type of cross section, as shown in Fig.23, and on the type of planform, as shown in Fig.24.

As a by-product of the analysis, we have obtained experimental values for the lift-dependent drag factor K , at small values of the lift coefficient (see Appendix D). For a fixed value of βs , the lift-dependent drag factor of delta wings decreases with increasing aspect ratio, as shown in Fig.27. For wings with the same type of cross-section shape, the values of K are independent of the thickness of the wing, but there is a small dependence on the type of cross section, as shown in Fig.28. At a given Mach number, the drag factor of a gothic wing, of aspect ratio $A = 1$, is about 0.2 lower than for a delta wing of the same aspect ratio, as shown in Fig.29.

Appendix A

THE ZERO-LIFT WAVE DRAG ACCORDING TO LINEAR THEORY

A theoretical estimate for the zero-lift wave drag is usually derived by means of the so-called supersonic area rule. The rule is based on linearized thin-wing theory. One assumes that the flow is inviscid and isentropic. The differential equation for the velocity potential ϕ is approximated by the linear equation

$$(M^2 - 1)\frac{\partial^2\phi}{\partial x^2} + \frac{\partial^2\phi}{\partial y^2} + \frac{\partial^2\phi}{\partial z^2} = 0 \quad . \tag{A-1}$$

The boundary condition that the flow is tangent to the wing surface is approximated by neglecting all second and higher order terms and by replacing it by a condition in the chordal plane of the wing, $z = 0$. Finally, the pressure coefficient is derived from the linearized Bernoulli equation

$$C_{p_\ell}(x,y) = -2\frac{v_x(x,y,0)}{V_0} \quad , \tag{A-2}$$

where $v_x(x,y,0)$ is the streamwise component of the perturbation velocity in the plane $z = 0$ and V_0 is the velocity of the undisturbed main stream.

It can be shown (see e.g. Ref.9) that the drag derived by integrating the pressure coefficient C_{p_ℓ} can also be obtained from the relation:

$$\frac{D_{w_\ell}(\beta)}{\frac{1}{2}\rho_0 V_0^2} = \frac{2}{\pi}\int_0^{\pi/2} d\theta \left\{ -\frac{\ell^2(\beta,\theta)}{2\pi}\int_0^1\int_0^1 \frac{d^2\left(\frac{S^*(x,\beta,\theta)}{\ell^2}\right)}{d\left(\frac{x}{\ell}\right)^2}\frac{d^2\left(\frac{S^*(x',\beta,\theta)}{\ell^2}\right)}{d\left(\frac{x'}{\ell}\right)^2} \log\left|\frac{x}{\ell} - \frac{x'}{\ell}\right| d\left(\frac{x}{\ell}\right) d\left(\frac{x'}{\ell}\right) \right\} \quad . \tag{A-3}$$

For wings and for given β and θ, $S^*(x,\beta\ \theta)$ is the projection into the plane x = constant of the cross sectional area intercepted by the plane through the point $(x,0,0)$ which is normal to the chordal plane of the wing and which makes with the free stream direction the angle $\cot^{-1}(\beta\cos\theta)$, see Fig.25. $\ell(\beta,\theta)$ is the interval of x over which the cross sectional area varies.

Fig.25 applies to wings with subsonic leading edges, for which $\beta\left(\frac{ds(x)}{dx}\right)_{max} < 1$; $|y| = s(x)$ describes the planform and $(ds(x)/dx)_{max}$ is the maximum value of $ds(x)/dx$. For subsonic leading edges $S^*(x,\beta,\theta)$ is zero in front of the apex, i.e. for $x < 0$; but when $\beta(ds(x)/dx)_{max} > 1$ the projected area may be non-zero for negative values of x, see Fig.26. With supersonic leading edges the position of the most forward point for which $S^*(x,\beta,\theta) \neq 0$ depends on the planform and on the value of $\beta s \cos\theta$.

To simplify some formulae, we restrict the discussion at first to wings with subsonic leading edges. At the end of this Appendix we state which formulae have to be modified to deal with supersonic leading edges.

We note that using the supersonic area rule for wing-body combinations implies the assumption that the interference velocity is negligible, i.e. one assumes that the perturbation velocity is equal to the sum of the velocity of the isolated exposed wing and the perturbation velocity of the isolated body.

In the following, we describe how the triple integral has been evaluated. We consider only configurations with unswept trailing edges. All lengths are made non-dimensional by taking the wing chord c_0 as unity. The notation

$$b = \beta s \cos\theta \tag{A-4}$$

is introduced, where s is the semispan of the wing at the trailing edge; then

$$\ell = \ell(\beta,\theta) = 1 + b \quad . \tag{A-5}$$

Instead of x we use the coordinate

$$\xi = \frac{x}{\ell(\beta,\theta)} = \frac{x}{1+b} \quad , \tag{A-6}$$

and we introduce the notation

$$S(\xi,b) = S(\xi,\beta,\theta) = \frac{S^*[x = \xi(1+b),\beta,\theta]}{\ell^2(\beta,\theta)} \quad . \tag{A-7}$$

To determine $S(\xi,\beta,\theta)$ for given β and θ we integrate the local thickness of the configuration along the straight line

$$y' = \frac{x - x'}{\beta \cos \theta} = s \frac{x - x'}{b} \quad . \tag{A-8}$$

The projection of this area into a plane normal to the x-axis is then given by

$$S^*(x,\beta,\theta) = 2 \int_{y_2}^{y_1} z(x',y')dy' \quad , \tag{A-9}$$

where

$$y_1 = s(x_1) = s \frac{x - x_1}{b} \tag{A-10}$$

and

$$\left.\begin{aligned} &\text{for } x < 1 - b: \quad y_2 = -s(x_2) = -s \frac{x_2 - x}{b} \\ &\text{for } 1 - b < x: \quad x_2 = 1, \quad y_2 = -s \frac{1 - x}{b} \quad . \end{aligned}\right\} \tag{A-11}$$

For a wing with a cylindrical sting of radius $R(= R/c_0)$, we write this relation in the form

$$\begin{aligned} S^*(x,\beta,\theta) &= -2 \int_{x_1}^{x_{1J}} z(x',y') \frac{dy'}{dx'} dx' - 2 \int_{x_{2J}}^{x_2} z(x',y') \frac{dy'}{dx'} dx' \\ &\quad + 2 \int_{y_{1J}}^{y_{2J}} \sqrt{R^2 - y'^2}\, dy' \\ &= \frac{2s}{b} \int_{x_1}^{x_{1J}} z(x',y')dx' + \frac{2s}{b} \int_{x_{2J}}^{x_2} z(x',y')dx' + 2 \int_{y_{1J}}^{y_{2J}} \sqrt{R^2 - y'^2}\, dy' \end{aligned} \tag{A-12}$$

(x_{1J},y_{1J}) and (x_{2J},y_{2J}) are the points where the line $y' = \frac{s}{b}(x - x')$ crosses the junction between sting and wing; forward of the sting

$x_{1J} = x_{2J} = x$, $y_{1J} = y_{2J} = 0$. To determine values for x_{1J} and x_{2J} as functions of x and b , one has to solve implicit equations, which can be done by iteration.

For delta wings with rhombic cross-sections, where the centre section is given by a polynomial in x , the integral $\int_{x_1}^{x_{1J}} z(x',y')dx'$ can be expressed by polynomials in x_1 and x_{1J} ; the limits x_1 and x_2 have the values

$$0 < \xi < \frac{1-b}{1+b}: \qquad x_1 = \xi$$

$$x_2 = \frac{1+b}{1-b}\,\xi$$

$$\frac{1-b}{1+b} < \xi < 1: \qquad x_1 = \xi$$

$$x_2 = 1 \quad .$$

When the tips are modified such that they are of conical shape, then it is also possible to express the integral $\int z(x',y')dx'$ in analytical form. For the wings of non-rhombic cross section, we have determined values of $S^*(x,\beta,\theta)$ by numerical integration.

For $b \neq 0$, values of the double integral

$$F(b) = -\frac{1}{2\pi}\int_0^1\int_0^1 S''(\xi,b)S''(\xi',b)\log|\xi-\xi'|d\xi d\xi' \quad , \qquad \text{(A-13)}$$

with $S''(\xi,b) = \frac{d^2S(\xi,b)}{d\xi^2}$, can be calculated by Eminton's technique[4]. We have applied the method using the values of $S(\xi,b)$ at the 40 equidistant positions $\xi_i = i/40$, $i = 1, 2, \ldots 40$.

The function $F(b)$ tends to infinity when b tends to zero, i.e. when θ tends to 90°. It has been shown in Ref.10 that for delta wings for which the thickness distributions behave near the trailing edge like

$$z(x,y) = x(1-x)\sum_{n=0}^{N} A_n(1-x)^n\left[1-\frac{|y|}{sx}\right] \quad , \qquad \text{(A-14)}$$

the function $F(b)$ behaves for small values of b as

$$F(b) = -\frac{1}{2\pi}\int_0^1\int_0^1 S''(x,b=0)S''(x')\log|x-x'|dxdx'$$

$$+\frac{1}{\pi}S'(1)\int_0^1 S''(x)\log(1-x)dx - \frac{1}{2\pi}[S'(1)]^2[\log b + 2 - k]$$

$$+ O(b\log b) + O(b) \qquad \text{(A-15)}$$

$S(x)$ is the area distribution in sections normal to the stream, $S'(1)$ is the first derivative of $S(x)$ at the trailing edge, and k is a constant which depends on the geometry near the trailing edge, see Ref.11 and Appendix B. Using equations (A-3), (A-15) and the relation

$$\frac{2}{\pi}\int_0^{\pi/2}\log\cos\theta\, d\theta = -\log 2 \quad , \qquad \text{(A-16)}$$

we obtain for small values of βs, i.e. small values of b for all values of θ :

$$\frac{D_{w_\ell}(\beta)}{\frac{1}{2}\rho_0 V_0^2} = -\frac{1}{2\pi}\int_0^1\int_0^1 S''(x)S''(x')\log|x-x'|dxdx'$$

$$+\frac{1}{\pi}S'(1)\int_0^1 S''(x)\log(1-x)dx + \frac{1}{2\pi}[S'(1)]^2[k - \log\beta s]$$

$$+ O(\beta s\log\beta s) + O(\beta s) \quad . \qquad \text{(A-17)}$$

This equation agrees for $\beta s \to 0$ with the drag from slender-body theory:

$$\frac{D_{w_s}(\beta)}{\frac{1}{2}\rho_0 V_0^2} = -\frac{1}{2\pi}\int_0^1\int_0^1 S''(x)S''(x')\log|x-x'|dxdx'$$

$$+\frac{1}{\pi}S'(1)\int_0^1 S''(x)\log(1-x)dx + \frac{1}{2\pi}[S'(1)]^2[k-\log\beta s] \quad . \quad (A\text{-}18)$$

Since $F(b)$ tends to infinity as $-\frac{1}{2\pi}[S'(1)]^2\log b$ when b tends to zero, we have, using equation (A-16), written equation (A-3) in the form

$$\frac{D_{w_\ell}(\beta)}{\frac{1}{2}\rho_0 V_0^2} = \frac{2}{\pi}\int_0^{\pi/2} H(b)d\theta + \frac{1}{2\pi}[S'(1)]^2[\log 2 - \log\beta s] \quad , \quad (A\text{-}19)$$

where for $b \neq 0$

$$H(b) = -\frac{\ell^2(b)}{2\pi}\int_0^1\int_0^1 S''(\xi,b)S''(\xi',b)\log|\xi-\xi'|d\xi d\xi' + \frac{1}{2\pi}[S'(1)]^2\log b \quad (A\text{-}20)$$

and for $b = 0$

$$H(b) = -\frac{1}{2\pi}\int_0^1\int_0^1 S''(x)S''(x')\log|x-x'|dxdx' + \frac{1}{\pi}S'(1)\int_0^1 S''(x)\log(1-x)dx$$

$$+\frac{1}{2\pi}[S'(1)]^2[k-\log 2] \quad . \quad (A\text{-}21)$$

Eminton's technique for evaluating the double integral is applicable when $S'(\xi = 1,b) = 0$. Since $S'(x = 1, b = 0) \neq 0$ we have used the extension of Eminton's technique given in Ref.12.

To perform the integration of $H(b = \beta s\cos\theta)$ with respect to θ , we have introduced the variable

$$\tau = \cos\theta = \frac{b}{\beta s} \quad . \quad (A\text{-}22)$$

Equation (A-19) can then be written in the form

$$\frac{D_{w_\ell}(\beta)}{\frac{1}{2}\rho_0 V_0^2} = \frac{2}{\pi}\int_0^1 \left[H(b = \beta s\tau) - H(b = \beta s)\right]\frac{d\tau'}{\sqrt{1-\tau^2}} + H(b = \beta s) + \frac{1}{2\pi}\left[S'(1)\right]^2\left[\log 2 - \log \beta s\right] \quad . \tag{A-23}$$

The integrand is everywhere finite since

$$\lim_{\tau \to 1} \frac{H(b = \beta s\tau) - H(b = \beta s)}{\sqrt{1-\tau^2}} = 0 \quad .$$

Equation (A-23) shows that for wings of different aspect ratio but with the same type of thickness distribution the drag is a function of the product βs only. However, if a sting with the same diameter $2R/c_0$ is added to wings of different span then the drag is a function of both β and s/c_0 .

For the delta wings without tip modification, the thickness distributions are of the type given by equation (A-14); but for the delta wings with modified tips the second derivative $S''(x)$ tends logarithmically to infinity when x tends to 1. The singularity of $S''(x \to 1)$ is related to the fact that the second derivative $\partial^2 z(x,y)/\partial x^2$ is finite for $|y| < sx$ but behaves like $1/(1 - x)$ for $y = sx$. For wings with streamwise tips and tip modifications similar to the type used for the delta wings, the second derivative $S''(x = 1)$ is finite.

It is not yet known whether, for wings for which $S''(x \to 1)$ tends to infinity, the function $F(b)$ behaves for small values of b as given by equation (A-15). We have nevertheless computed values of $H(b)$ as defined by equations (A-20), (A-21). For determining the double integral in equation (A-21), we have again used the extension of Eminton's technique given in Ref.12, but we have not examined the accuracy of the results for cases where $S''(x \to 1)$ tends to infinity. To evaluate the single integral in equation (A-21) we have somewhat modified the method of Ref.12 by, subtracting from $S(x)$ a term whose second derivative has the known singular behaviour of $S''(x \to 1)$.

For the delta wings with modified tips, it was found that the values of $H(b)$ computed for $b = 0$ differ appreciably from those computed for small but

non-zero values of b, in contrast to the results for the wings without tip modification. However, when the computed values of $H(b)$ are plotted against $b \log b$, it is found that the values vary nearly linearly. This numerical result has been interpreted as implying that equations (A-15) and (A-17) still apply when $S''(x \to 1)$ tends logarithmically to infinity.

When slender-body theory is used to estimate the wave drag for non-zero values of βs, the tacit assumption is made that in equation (A-17) the term which behaves like $\beta s \log \beta s$ is small. When this assumption does not hold, as for the delta wings with modified tips, then slender-body theory is of no use even for values of βs which would usually be considered small, say $\beta s < 0.2$. As stated above, we do not expect a similar difficulty to arise for wings with streamwise tips.

To evaluate the effect of the tip modification on the wave drag, we have not used equation (A-23) for the wings with modified tips, but have evaluated the change in drag ΔD_{w_ℓ} from the relation

$$\frac{\Delta D_{w_\ell}}{\frac{1}{2}\rho_0 V_0^2} = \frac{2}{\pi} \int_0^{\pi/2} \ell^2(b) \Delta F(b = \beta s \cos\theta) d\theta \quad , \qquad \text{(A-24)}$$

where ΔF is the difference between the values of $F(b)$ computed for the configurations with modified wing tips and those computed for the basic wings. The values of $\Delta F(b)$ are small except for small values of b. For the computation of ΔD_{w_ℓ} we have written equation (A-24) in the form:

$$\frac{\Delta D_{w_\ell}}{\frac{1}{2}\rho_0 V_0^2} = \frac{2}{\pi} \int_0^{\psi} \ell^2(b) \Delta F(b = \beta s \cos\theta) d\theta + \frac{2}{\pi} \int_{\psi}^{\pi/2} \Delta H(b = \beta s \cos\theta) d\theta$$

$$- \frac{2}{\pi} \frac{[S'(1)]^2_{mod} - [S'(1)]^2_{bas}}{2\pi} \left[\left(\frac{\pi}{2} - \psi \right) \log \beta s + \int_{\psi}^{\pi/2} \log \cos\theta \, d\theta \right] \quad ,$$

.....(A-25)

where $S'(1)_{mod}$ and $S'(1)_{bas}$ are the derivatives of the area distributions for the configurations with and without modified wing tips and ψ is chosen close to $\pi/2$.

The integrals have been obtained graphically except the integral $\int_{\psi}^{\pi/2} \log \cos\theta \, d\theta$, for which numerical values are given in Table 1 of Ref.13. In addition to the computed values of $H(b)$ we have, for small values of b, interpolated some further values by plotting the computed values of $H(b)$ against $b \log b$ and against b.

We also need to evaluate the drag from equation (A-3) for wings with supersonic leading edges. For model 238, where $s(x) = \frac{1}{3} x(2 - x)$ i.e. $(ds(x)/dx)_{max} = 2/3$, the leading edge is supersonic at the apex for $\beta > 3/2$, i.e. $M > 1.80$.

When for some negative values of x the area $S^*(-|x|,b) \neq 0$, then we have to modify equations (A-5) and (A-6). We denote by $x = -x^*(b)$ the coordinate of the most forward point for which $S^* \neq 0$; then

$$\ell(b) = 1 + b + x^*(b) \tag{A-5a}$$

and

$$\xi = \frac{x + x^*(b)}{\ell(b)} \quad . \tag{A-6a}$$

Equation (A-7) is therefore to be modified to

$$S(\xi,b) = \frac{S^*(x = \xi\ell(b) - x^*(b);b)}{\ell^2(b)} \tag{A-7a}$$

For $-x^* < x < 0$, equation (A-10) has to be modified to

$$y_1 = -s(x_1) = s\frac{x - x_1}{b} \quad ; \tag{A-10a}$$

equation (A-11) applies to the interval $-x^* < x < 1 - b$.

For model 238 and $b > 0.5$,

$$x^* = \frac{(2b - 1)^2}{4b}$$

$$\ell(b) = \frac{1 + 8b^2}{4b}$$

$$-\frac{(2b-1)^2}{4b} < x < 0 \quad : \quad x_1 = \frac{1}{2b}\left[2b - 1 - \sqrt{(2b-1)^2 + 4bx}\right]$$

$$0 < x < 1 + b \quad : \quad x_1 = \frac{1}{2b}\left[2b + 1 - \sqrt{(2b+1)^2 - 4bx}\right]$$

$$-\frac{(2b-1)^2}{4b} < x < 1 - b \quad : \quad x_2 = \frac{1}{2b}\left[2b - 1 + \sqrt{(2b-1)^2 + 4bx}\right] \quad .$$

For delta wings, the area distribution $S(\xi, b = 1)$, i.e. the area distribution generated by cuts parallel to one of the leading edges, has the special feature that the first derivative is finite at the apex, $S'(\xi = 0, b = 1) \neq 0$. We have not yet extended Eminton's technique for evaluating $F(b)$, equation (A-13), to cases for which $S'(0) \neq 0$, so that we cannot evaluate $F(b = 1)$ nor D_{w_ℓ} for values of $\beta s \geq 1$. For a delta wing of simple geometry, e.g. with double wedge sections, the pressure distribution according to linear theory can be determined analytically, see e.g. Refs.14 and 15. The integrated pressure drag is finite at $\beta s = 1$, but the curve of $C_{D_{0w}}$ against βs has a discontinuous slope at $\beta s = 1$. This discontinuity is a consequence of the assumption made in linear theory that all disturbances of the flow are propagated within cones of the same Mach angle $\mu = \tan^{-1} \beta$. In reality the local Mach number is not constant and therefore the drag computed by a non-linear theory and the experimental drag vary smoothly near $\beta s = 1$.

For wings with curved planforms, where $S'(\xi = 0, b = 1) = 0$, the evaluation of $F(b = 1)$ and therefore of $D_{w_\ell}(\beta s \geq 1)$ does not cause any difficulty.

Appendix B

EVALUATION OF THE CONSTANT k IN EQUATION (A-15)

The constant k in equation (A-15) depends on the geometry of the configuration at the trailing edge. For the case of a wing with an unswept trailing edge attached to a circular cylindrical body in a midwing position, Lighthill[11] has shown, see also Ref.16, that k can be determined from the relation

$$k = \log 2 - \frac{\int_R^s \int_R^s \varepsilon(y)\varepsilon(y') \left\{ \log \left| \frac{y^2}{s^2} - \frac{y'^2}{s^2} \right| + \log \left[1 - \frac{R^4}{y^2 y'^2} \right] \right\} dy'dy}{2 \left[\int_R^s \varepsilon(y)dy \right]^2} \qquad \text{(B-1)}$$

where R is the radius of the body and

$$\varepsilon(y) = \left[\frac{\partial z(x,y)}{\partial x} \right]_{x=1}$$

is the slope of the upper surface of the wing at the trailing edge. With the notation

$$\tau = \frac{y - R}{s - R}$$

$$\alpha = \frac{R}{s - R}$$

equation (B-1) can be written in the form

$$k = \log 2 + \log (1 + \alpha) - \frac{\int_0^1 \varepsilon(\tau) \int_0^1 \varepsilon(\tau') \left\{ \log \left| (\tau + \alpha)^2 - (\tau' + \alpha)^2 \right| + \log \left[1 - \frac{\alpha^4}{(\tau+\alpha)^2 (\tau'+\alpha)^2} \right] \right\} d\tau' d\tau}{2 \left[\int_0^1 \varepsilon(\tau)d\tau \right]^2}$$

..... (B-2)

In order to evaluate k numerically, it is advisable to extract the singular part of the integrand. Since

$$\int_0^1 \log\left|(\tau+\alpha)^2 - (\tau'+\alpha)^2\right| d\tau' = (1-\tau)\log(1-\tau) + \tau\log\tau + (1+\tau+2\alpha)\log(1+\tau+2\alpha) - (\tau+2\alpha)\log(\tau+2\alpha) - 2$$

and

$$\int_0^1 \log\left[1 - \frac{\alpha^4}{(\tau+\alpha)^2(\tau'+\alpha)^2}\right] d\tau'$$

$$= \left(1 + \frac{\alpha\tau}{\tau+\alpha}\right)\log\left(1 + \frac{\alpha\tau}{\tau+\alpha}\right) - \frac{\alpha\tau}{\tau+\alpha}\log\frac{\alpha\tau}{\tau+\alpha}$$

$$+ \left(1 + \frac{\alpha\tau + 2\alpha^2}{\tau+\alpha}\right)\log\left(1 + \frac{\alpha\tau + 2\alpha^2}{\tau+\alpha}\right) - \frac{\alpha\tau + 2\alpha^2}{\tau+\alpha}\log\frac{\alpha\tau + 2\alpha^2}{\tau+\alpha} - 2(1+\alpha)\log(1+\alpha) + 2\alpha\log\alpha$$

we write equation (B-2) in the form

$$k = \log 2 + \log(1+\alpha)$$

$$- \frac{1}{2\left[\int_0^1 \varepsilon(\tau)d\tau\right]^2} \int_0^1 \varepsilon(\tau)\left[\int_0^1 \{\varepsilon(\tau') - \varepsilon(\tau)\}\left\{\log\left|(\tau+\alpha)^2 - (\tau'+\alpha)^2\right| + \log\left[1 - \frac{\alpha^4}{(\tau+\alpha)^2(\tau'+\alpha)^2}\right]\right\} d\tau'\right.$$

$$\left. + \varepsilon(\tau)\left\{(1-\tau)\log(1-\tau) + \tau\log\tau + (1+\tau+2\alpha)\log(1+\tau+2\alpha)\right.\right.$$

$$\left.\left. - (\tau+2\alpha)\log(\tau+2\alpha) - 2 + \left(1 + \frac{\alpha\tau}{\tau+\alpha}\right)\log\left(1 + \frac{\alpha\tau}{\tau+\alpha}\right)\right.\right.$$

$$- \frac{\alpha\tau}{\tau + \alpha} \log \frac{\alpha\tau}{\tau + \alpha} + \left(1 + \frac{\alpha\tau + 2\alpha^2}{\tau + \alpha}\right) \log \left(1 + \frac{\alpha\tau + 2\alpha^2}{\tau + \alpha}\right)$$

$$- \frac{\alpha\tau + 2\alpha^2}{\tau + \alpha} \log \frac{\alpha\tau + 2\alpha^2}{\tau + \alpha} - 2(1 + \alpha) \log (1 + \alpha) + 2\alpha \log \alpha \Big\} \Big] \, d\tau \, . \quad \text{(B-3)}$$

For a wing without a body, for which $\varepsilon(y)$ varies linearly over the inner part of the wing, i.e.

$$\varepsilon(y) = \varepsilon(0) \left[1 - \left|\frac{y}{s}\right|\right] \quad , \qquad 0 < \left|\frac{y}{s}\right| < a$$

and $\varepsilon(y)$ is constant for the outer part of the wing,

$$\varepsilon(y) = \varepsilon(0)(1 - a) \quad , \qquad a < \left|\frac{y}{s}\right| < 1$$

one can derive an analytic expression for k :

$$k = \log 2 - \frac{2}{\left[1 + (1 - a)^2\right]^2} \left\{ \frac{(1 - a)(1 + a)^3}{3} \log (1 + a) + \frac{(1 - a)^4}{3} \log (1 - a) + \frac{a^4}{2} \log a \right.$$

$$\left. + \left[2(1 - a)^2 + \frac{2a^4}{3}\right] \log 2 - (1 - a)\left(3 - 3a + \frac{11}{3} a^2\right) - \frac{25}{24} a^4 \right\} \quad . \qquad \text{(B-4)}$$

This relation contains the two results

$$a = 0 \, , \qquad k = 3/2$$

$$a = 1 \, , \qquad k = \frac{25}{12} - \frac{1}{3} \log 2 \quad ,$$

given in Ref.16. We quote the values computed for the wing of model 229, with and without the sting shroud and the tip modification.

	a	R/s	k
basic wing	1	0	1.852
basic wing	1	0.0625	1.800
modified wing	0.65	0	1.684
modified wing	0.65	0.0625	1.632

Appendix C

DERIVATION OF THE ZERO-LIFT DRAG FROM BALANCE MEASUREMENTS

The tabulated results from the balance tests do not include values for the drag coefficient at the incidence for which the lift is exactly zero. Further the $C_D(C_L)$ curves are not exactly symmetrical with respect to $C_L = 0$. Such an asymmetry may be caused by some non-uniformity of the flow in the empty tunnel or by some asymmetry of the model. To eliminate the main effects of flow deflection, one would nowadays test the model also in the inverted position. This was not done in these early tests. The $C_D(C_L)$ curves are similar to those of slightly cambered wings.

To derive an approximate value for the zero-lift drag of the symmetrical wing in uniform parallel flow, we have expressed $C_D(C_L)$ in the form suggested by linear theory for a cambered wing:

$$C_D = C_{D\,min} + \frac{K}{\pi A} (C_L - C_{L\,min})^2 \quad . \qquad (C\text{-}1)$$

The drag factor is of course a function of C_L, partly because the leading edge vortices produce non-linear effects and also because the friction drag is not strictly independent of C_L. However, for a small incidence range (say $|\alpha| < 3^o$), equation (C-1) with constant values of K, $C_{L\,min}$ and $C_{D\,min}$ may be an adequate representation. Our aim is then to find values of $C_{L\,min}$ and K such that, for $|\alpha| < 3^o$, the corresponding values of

$$C_{D\,min} = C_D - \frac{K}{\pi A} (C_L - C_{L\,min})^2$$

are independent of C_L, within the accuracy to be expected of the measurements. It proved possible to find values of $C_{L\,min}$ and K such that the variation in $C_{D\,min}$ was small and random over the incidence range; the mean of these values of $C_{D\,min}$ has been taken.

It was found that for most cases $|C_{L\,min}| \leqslant 0.002$. (For two test runs with model 233: $C_{L\,min} = -0.004$.) (When one examines how the values of $C_{L\,min}$ vary with Mach number for the various models, it seems likely that the asymmetry of the $C_D(C_L)$ curves is produced partly by a non-uniform flow and partly by some small asymmetry of the models.)

Since the values of $C_{L\ min}$ are small and $K/\pi A < 1$, we consider the term $C_{D\ min}$ to be a reasonably accurate estimate of the zero-lift drag coefficient for the symmetrical configuration.

The procedure was not always quite straightforward. For Mach numbers $M \geqslant 2.4$, the values of $C_{D\ min}$ derived from the measured values of $C_D(C_L)$ for $|C_L|$ close to zero are in some cases smaller than the values derived for say $|C_L| > 0.03$. These smaller values may be a consequence of somewhat ineffective transition strips. When such a 'laminar bucket' was obvious, the low values of $C_{D\ min}$ were excluded from the derivation of the mean value. (It is unfortunate that the forces were measured at wider intervals of the angle of incidence than would be used today.)

With a test run at any particular Mach number the scatter of the $C_{D\ min}$ values is less than 0.0002 and the uncertainty caused by incomplete transition seems to be smaller than 0.0002.

With respect to the accuracy of the balance measurements of the drag, A.O. Ormerod has contributed the following note.

In the results from overall force measurements there was uncertainty because of the unknown drift of the balance readings corresponding to zero aerodynamic load. The results were computed with the assumption that the zero readings varied linearly with time from those observed before the run to those observed after the run. The few repeat tests made during this series and subsequent experience have shown that this assumption was not entirely satisfactory. It is considered that the resulting uncertainty in drag measurement, applicable to all the tests in this Report, was ±0.7 lb(±3N). For the delta wings of aspect ratio 4/3 this corresponded to ±0.0002 in drag coefficient at Mach numbers between 1.4 and 2.4 and to ±0.0003 at Mach numbers of 2.6 and 2.8. For other wings the uncertainty in terms of drag coefficient was inversely proportional to the plan area.

Appendix D

EXPERIMENTAL RESULTS FOR THE LIFT-DEPENDENT DRAG FACTOR

The values of the lift-dependent drag factor K for small values of $|C_L|$, $|\alpha| < 3^o$, which were derived from the present tests on delta wings with rhombic cross sections are plotted in Fig.27. We have also plotted the curves, derived by linear theory, for thin, uncambered delta wings, both with and without leading-edge suction (with full leading-edge suction $K = 2E(k) - k$, where $k^2 = 1 - \beta^2 s^2$; with no leading-edge suction $K = 2E(k)$ where E is the complete elliptic integral of the second kind). We may note that four wings of aspect ratio 4/3 with rhombic cross sections were tested; three of these wings had the same type of thickness distribution but the thickness-to-chord ratio varied (between 6% and 11%). Within the accuracy of the K-values, say $|\Delta K| < 0.05$, the K-values were independent of the wing thickness. One may perhaps interpret this fact as implying that the aeroelastic distortion of the wings which was known to occur has not had a large effect on the K-values at small values of the lift coefficient.

For the delta wings of different cross-sectional shapes (with the same aspect ratio and the same area distribution) we found some systematic dependence of the K-values on the type of section shape. We have plotted the results in Fig.28. As we should expect, the values of K for the round-edged wing are lower than those for the sharp-edged wings at these low lift coefficients, since some leading-edge suction will be realised. It is not clear why the rhombic cross sections should be superior to the parabolic sections of the same area. In general for sharp-edged wings two effects oppose one another: greater thickness reduces the circulation in the leading-edge vortex sheet, see Ref.17, but also provides more forward facing surface for the suction peak to act on.

The K-values obtained for the wing with a gothic planform are plotted in Fig.29 as a function of $\frac{1}{4}\beta A$, following the procedure of Ref.18. The figure contains also the K-values, from Fig.27, for the delta wing with the same aspect ratio, $A = 1$. We have also plotted the curves derived by linear theory for no leading-edge suction. Values of K for the gothic planform have been computed by P.J. Davies (RAE, unpublished) using a program developed by A. Roberts[19]. The values of K for the gothic wing are lower than those for the delta wing of the same aspect ratio.

Appendix E

ESTIMATE OF THE SKIN-FRICTION DRAG

A full scale boundary-layer calculation for the flow past a three-dimensional configuration is a formidable task. We therefore derive only an estimate for the skin-friction drag.

We take advantage of the fact that at zero lift the pressure gradients are small. Cooke[5] has shown that for fairly thin wings the effect on the boundary layer of the pressure gradients and the streamline curvature is negligible, so that the boundary layer develops along each chordline in the same way as the boundary layer over a semi-infinite plate at zero incidence having a leading edge normal to the incident stream. The local skin friction c_f at a point x, y depends then only on the chordwise distance of the point from the leading edge, $x - x_{le}(y)$, and the properties of the free stream.

It has become standard practice, see Smith[20], to take account of the difference between the wetted area of the actual wing and the planform area. Let us consider an element of the wing surface $z(x,y)$ of area $ds \times d\sigma$, with the plan area $dx \times dy$. The skin friction which acts on this element of the wing surface produces a tangential force of magnitude

$$c_f(x,y)ds d\sigma = c_f(x,y)\sqrt{1 + \left(\frac{\partial z}{\partial x}\right)^2}\,dx\sqrt{1 + \left(\frac{\partial z}{\partial y}\right)^2}\,dy \quad .$$

We assume that the inclination of this friction force to the x-direction is small, so that its drag component has the magnitude

$$c_f(x,y)ds d\sigma \frac{dx}{ds} = c_f(x,y)\sqrt{1 + \left(\frac{\partial z(x,y)}{\partial y}\right)^2}\,dx dy \quad .$$

Thus the coefficient of the skin-friction drag for a wing with an unswept trailing edge is calculated from

$$C_{D_F}\left(R_{C_0}\right) = 4\int_0^1 d\left(\frac{y}{s}\right)\int_{x_{le}(y)}^1 c_f\left[(x - x_{le}(y))R_{C_0}\right]\sqrt{1 + \left(\frac{\partial z(x,y)}{\partial y}\right)^2}\,dx \quad . \qquad \text{(E-1)}$$

$c_f\left[(x - x_{le}(y))R_{C_0}\right]$ is the local skin-friction coefficient, which is a function of the Reynolds number R_x based on the distance from the effective start of the boundary layer; we assume this is at the leading edge, so that $R_x = (x - x_{le}(y))R_{C_0}$, where R_{C_0} is the Reynolds number based on the wing chord, c_0.

For fully turbulent boundary layers, zero heat transfer and a tunnel total temperature between 0^oC and 60^oC, Smith[20] has produced diagrams for the mean skin friction coefficient

$$C_F(R_\ell;M) = \frac{1}{\ell}\int_0^\ell c_f(R_x;M)dx \quad . \tag{E-2}$$

Using these diagrams one can evaluate the drag coefficient of a flat plate from

$$C_{D_F \text{ flat plate}}\left(R_{C_0}, M\right) = 4\int_0^1 \frac{c(y)}{c_0} C_F\left(R_\ell = \frac{c(y)}{c_0} R_{C_0}; M\right) d\left(\frac{y}{s}\right) \tag{E-3}$$

where $c(y)$ is the local chord (for the delta planform: $c(y)/c_0 = 1 - y/s$, for the gothic planform: $c(y)/c_0 = \sqrt{1 - y/s}$). We note that the effect of the planform on C_{D_F} is small. For $R_{C_0} = 10^7$ and $1.4 \leqslant M \leqslant 2.4$ it was found that for the gothic planform the value of $C_{D_F \text{ flat plate}}$ is about 3% smaller than for the delta planform.

For wings for which the surface slopes are not large, equation (E-1) can be approximated by

$$C_{D_F} = C_{D_F \text{ flat plate}} \frac{\displaystyle\int_0^1 d\left(\frac{y}{s}\right) \int_{x_{le}(y)}^1 \sqrt{1 + \left[\frac{\partial z(x,y)}{\partial y}\right]^2}\, dx}{\displaystyle\int_0^1 \frac{c(y/s)}{c_0} d\left(\frac{y}{s}\right)}$$

$$= C_{D_F \text{ flat plate}} \frac{\displaystyle\int_0^1 dx \int_0^{s(x)} \sqrt{1 + \left[\frac{\partial z(x,y)}{\partial y}\right]^2}\, dy}{\displaystyle\int_0^1 s(x)dx} \quad . \tag{E-4}$$

For model 242, which has fairly large spanwise slopes over a large region of the plan area

$$\left|\frac{\partial z}{\partial y}\right| = 1.89(1 - x)(1 - 1.5x + x^2 - 0.25x^3) \quad ,$$

we have computed C_{D_F} both from equation (E-1) and from equation (E-4) for $R_{C_0} = 10^7$ and $M = 2$. Equation (E-1) gives for the ratio between the skin-friction drag for the thick wing and the flat plate the value 1.102, whilst equation (E-4) gives 1.089. In view of the other simplifying assumptions made in deriving equation (E-1) and the limited accuracy of the experimental results, we have used the simpler equation (E-4) in the present analysis. The effect of the sting shroud on C_{D_F} has been ignored.

We quote in the following table the values of the ratio between C_{D_F} and $C_{D_F \text{ flat plate}}$ used in the analysis.

Model	$\frac{C_{D_F}}{C_{D_F \text{ flat plate}}}$	ΔC_D roughness
229	1.024	0.00016
230	1.025	0.00016
231	1.018	0.00016
233	1.042	0.00016
234	1.025	0.00016
237	1.015	0.00012
238	1.008	0.00016
239	1.042	0.00021
240	1.015	0.00016
242	1.089	0.00030

When calculating $C_{D_F \text{ flat plate}}$ it was assumed that the flow was turbulent from the leading edge. To produce the transition to turbulent flow close to the leading edge transition strips were attached to all models near the leading edge. An allowance must be made for the drag of these roughness bands.

Several details of the transition strips are not known, so that we can make only a crude estimate for the drag increase caused by the transition strips.

Evans[21] has suggested that the increase in the friction-drag coefficient due to roughness bands is proportional to the ratio between the area of the roughness band and the reference wing area:

$$\Delta C_D = K \frac{\text{roughness band area}}{\text{reference wing area}} \quad . \qquad \text{(E-5)}$$

Using bands of 60 grade carborundum grit, which had been carefully sieved and sprinkled sparsely, he obtained for K the value 0.0032 and found that K is only weakly dependent on Mach number and Reynolds number over the range investigated, $1.4 < M < 2.6$; $10^7 < R_{C_0} < 2.10^7$.

With the tests discussed in this Report the roughness strips consisted of nominally 100 grade carborundum grit, but it may be assumed that the grit had not been carefully sieved, so that it would have contained some over-sized particles. It is now not known whether the carborundum grit was applied sparsely. The uncertainties of the geometrical details of the roughness bands imply that the estimate for the roughness drag is uncertain; we have used for the factor K in equation (E-5) the value 0.003.

The width of the roughness bands normal to the leading edge was 0.25in. Hence for the delta wings, with s and c_0 measured in inches:

$$\frac{\text{roughness band area}}{\text{planform area}} \approx 2 \times 2 \times \frac{0.25\sqrt{c_0^2 + s^2}}{sc_0}$$

$$= 4 \times \frac{0.25}{60} \sqrt{1 + \frac{1}{(s/c_0)^2}} \quad .$$

The values used in the analysis for the drag coefficient caused by the roughness bands are quoted in the table. We note that they are of a magnitude similar to that of the uncertainty in the balance measurements, $\Delta C_D = \pm 0.0002$.

Table 1

GEOMETRY OF DELTA AND GOTHIC WINGS TESTED IN THE 8ft × 8ft TUNNEL

Planform	Model number	Aspect ratio	$\frac{vol}{c_0^3}$	Cross section	Centre line section $z(x,0)/c_0$	Extent of tip modification* x_{le}/c_0	y_{te}/s
Delta	229	4/3	0.01	rhombic	$0.18x(1 - x)$	0.9	0.65
"	230	4/3	0.01	elliptic	$0.11459x(1 - x)$	no modification	
"	231	4/3	0.01	parabolic	$0.135x(1 - x)$	0.917	0.75
"	233	4/3	0.01	rhombic	$0.105x(1 - x)[4 - 6x + 4x^2 - x^3]$	0.833	0.45
"	234	4/3	0.0075	rhombic	$0.07875x(1 - x)[4 - 6x + 4x^2 - x^3]$	0.792	0.325
"	237	16/9	0.01	rhombic	as 234	0.75	0.375
"	239	1	0.00563	rhombic	as 234	0.817	0.233
"	240	4/3	0.00563	rhombic	$0.05906x(1 - x)[4 - 6x + 4x^2 - x^3]$	0.783	0.3
"	242	2/3	0.00375	rhombic	as 234	0.875	0.25
Gothic	238	1.0	0.01	rhombic	$0.105x(1 - x)[2 - 2x + x^2]$	0.85	0.65

All wings had the length c_0 = 60in (= 1.524m). x denotes x/c_0 .

* The wing thickness was increased in the region for which

$$\left|\frac{y}{s}\right| > \frac{x_{le}}{c_0} - \frac{\frac{x_{le}}{c_0} - \frac{y_{te}}{s}}{1 - \frac{x_{le}}{c_0}} \left(\frac{x}{c_0} - \frac{x_{le}}{c_0}\right)$$

SYMBOLS

A	aspect ratio
c_0	chord of centre section, taken as unity
$c(y)$	local chord
c_f	local skin-friction coefficient
c_p	pressure coefficient
C_D	drag coefficient
C_{D_0}	drag coefficient at zero lift
$C_{D_{0w}}$	coefficient of zero-lift wave drag
C_{D_F}	drag coefficient due to skin friction
C_L	lift coefficient
D	drag
D_w	wave drag
K	lift-dependent drag factor
K_0	zero-lift wave drag factor, see equation (2)
M	free-stream Mach number
R	radius of the sting shroud
R_{c_0}	Reynolds number based on the wing chord, c_0
$s(x)$	local semispan
s	$= s(x = 1)$, semispan at the trailing edge
$S(x)$	area distribution in sections normal to the stream
V_0	free stream velocity
x, y, z	rectangular coordinate system, x-axis coincides with the centre line of the wing
$z(x,y)$	wing ordinate
α	angle of incidence
β	$= \sqrt{M^2 - 1}$
2δ	$= 2 \tan^{-1} \lvert \partial z(x,y)/\partial y \rvert_{y=s(x)}$, edge angle of spanwise cross sections
ρ_0	density in free stream

Suffices

ℓ	derived by linear theory
mod	produced by tip modification
s	derived by slender-body theory

For notation used in Appendix A see Figs.25 and 26.

REFERENCES

No.	Author	Title, etc.
1	W.T. Lord G.G. Brebner	Supersonic flow past slender pointed wings with 'similar' cross sections at zero lift. Aero. Quart. 10, 79 (1959)
2	J.W. Britton	Pressure measurements at supersonic speeds on three uncambered conical wings of unit aspect ratio. ARC CP No.641 (1962)
3	J Weber	Slender delta wings with sharp edges at zero lift. RAE Technical Note Aero 2508 (ARC 19549) (1957)
4	E. Eminton	On the numerical evaluation of the drag integral. ARC R & M 3341 (1961)
5	J.C. Cooke	Turbulent boundary layers on delta wings at zero lift. ARC CP No.696 (1963)
6	J.C. Cooke	Slender not-so-thin wing theory. ARC CP No.659 (1962)
7	K.G. Smith L. Gaudet K.G. Winter	The use of surface pitot tubes as skin friction meters at supersonic speeds. ARC R & M 3351 (1962)
8	H.B. Squire	An example in wing theory at supersonic speed. ARC R & M 2549 (1951)
9	H. Lomax	The wave drag of arbitrary configurations in linearized flow as determined by areas and forces in oblique planes. NACA RM A55 A18 (1955)
10	J Weber	Some notes on the zero-lift wave drag of slender wings with unswept trailing edge. ARC R & M 3222 (1959)
11	M.J. Lighthill	The wave drag at zero lift of slender delta wings and similar configurations. J. Fluid Mech. 1, 337 (1956)
12	J. Weber	Numerical methods for calculating the zero-lift wave drag and the lift-dependent wave drag of slender wings. ARC R & M 3221 (1959)

REFERENCES (concluded)

No.	Author	Title, etc.
13	J.C. Cooke J.A. Beasley	Zero lift wave drag of slender wings with swept trailing edges. RAE Technical Note Aero 2699 (ARC 22281) (1960)
14	A.E. Puckett	Supersonic wave drag of thin airfoils. Jour. Aero. Scs., 13, 475 (1946)
15	A. Henderson	Supersonic wave drag of non-lifting delta wings with linearly varying thickness ratio. NACA Technical Note 2858 (1952)
16	J Weber	The effect of the geometry near the trailing edge on the zero-lift wave drag of slender wings. RAE Technical Note Aero 2662 (ARC 22147) (1960)
17	J.H.B. Smith	Calculations of the flow over thick, conical, slender wings with leading-edge separation. ARC R & M 3694 (1971)
18	A.L. Courtney	A collection of data on the lift-dependent drag of uncambered slender wings at supersonic speeds. ARC CP No.737 (1960)
19	A. Roberts	Thin supersonic wing program. BAC Aero MA Report 5 (1967)
20	K.G. Smith	Methods and charts for estimating skin friction drag in wind tunnel tests with zero heat transfer. ARC CP No.824 (1964)
21	J.Y.G. Evans	Transition fixing techniques and the interpretation of boundary layer conditions on slender wings in supersonic wind tunnels. RAE Technical Note Aero 2946 (ARC 25892) (1964)

Note: *References quoted are not necessarily available*

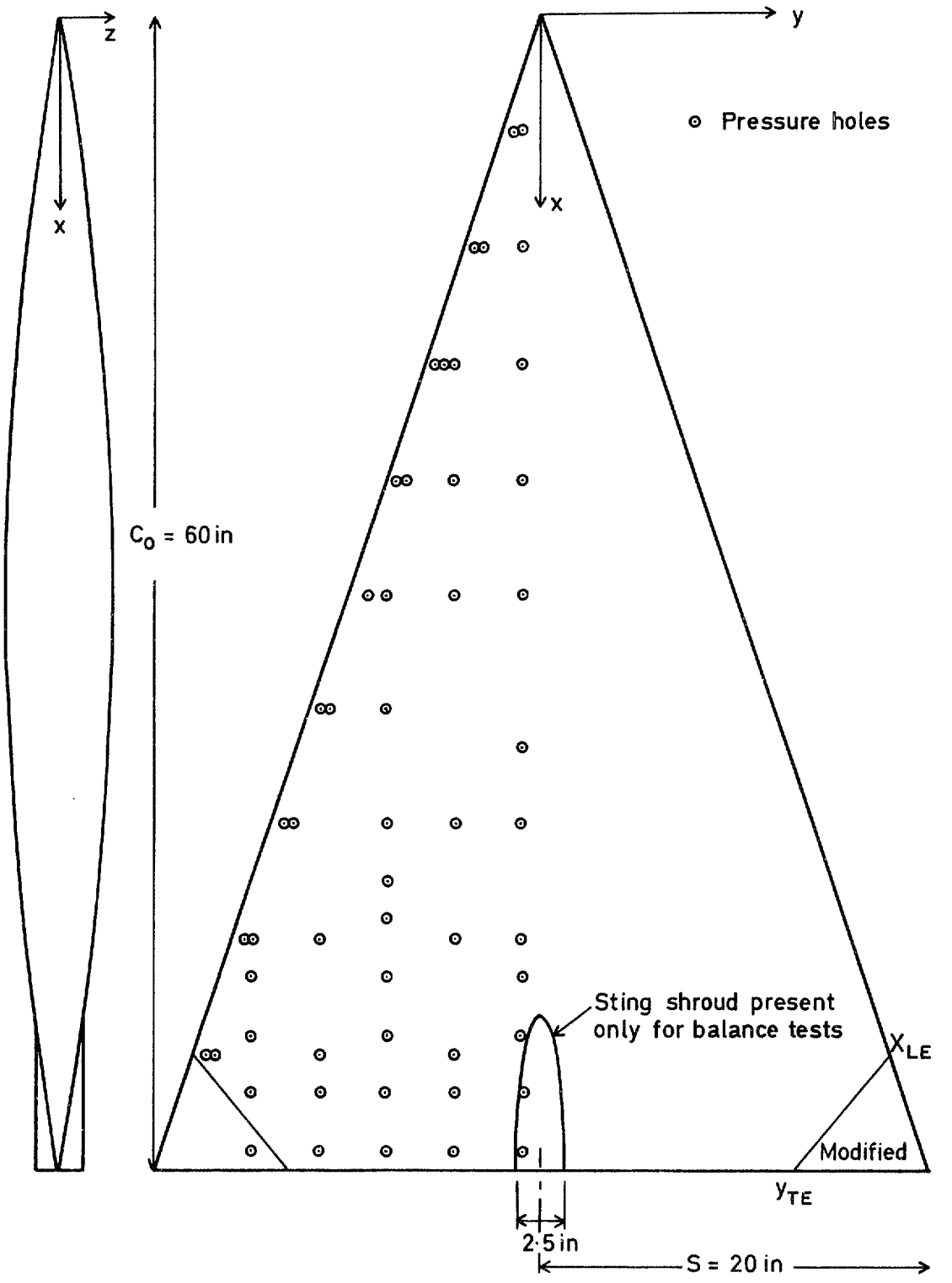

Fig.1 GA of model 229

Fig 2

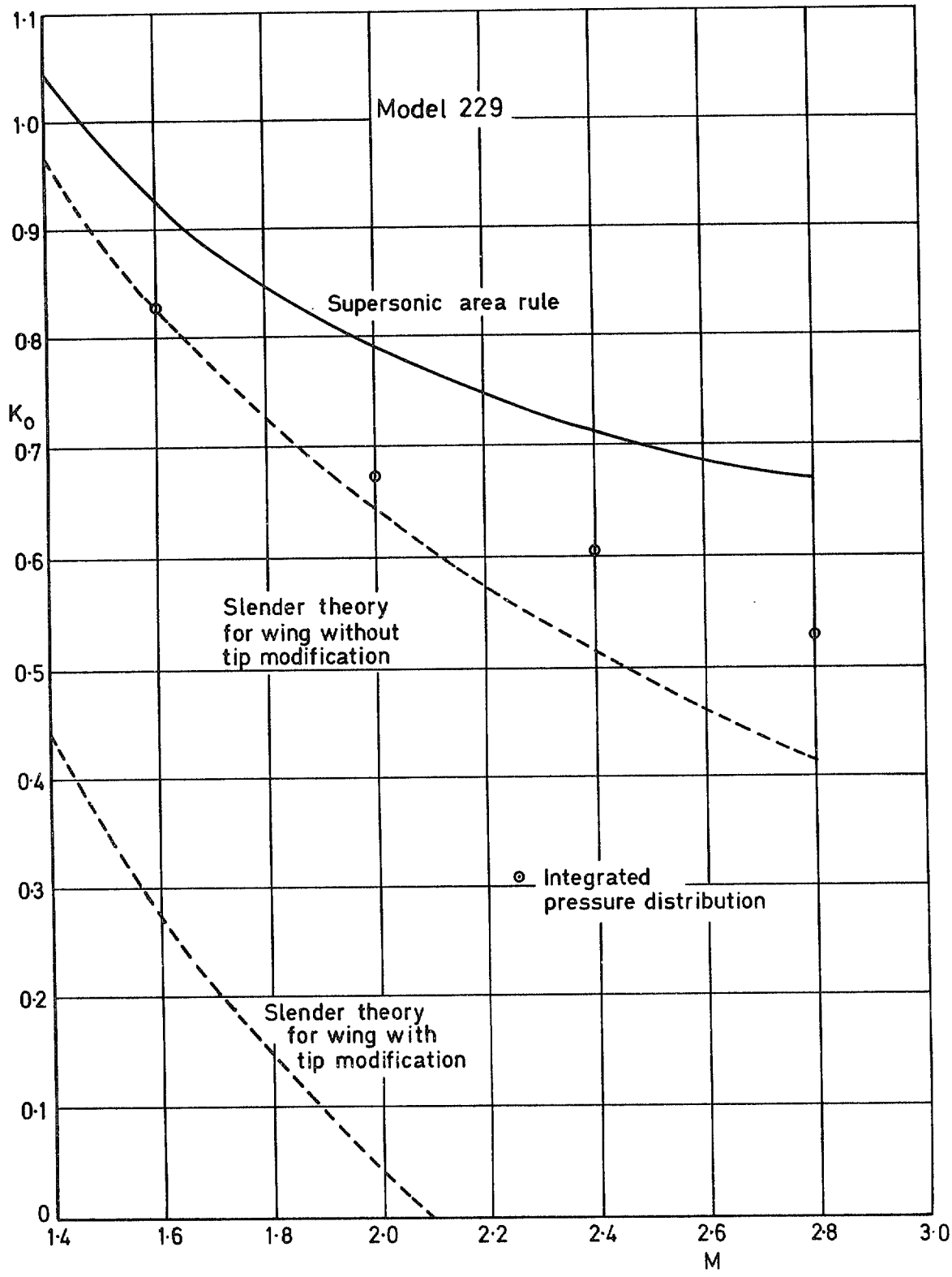

Fig.2 Zero-lift drag factor for wing without sting shroud

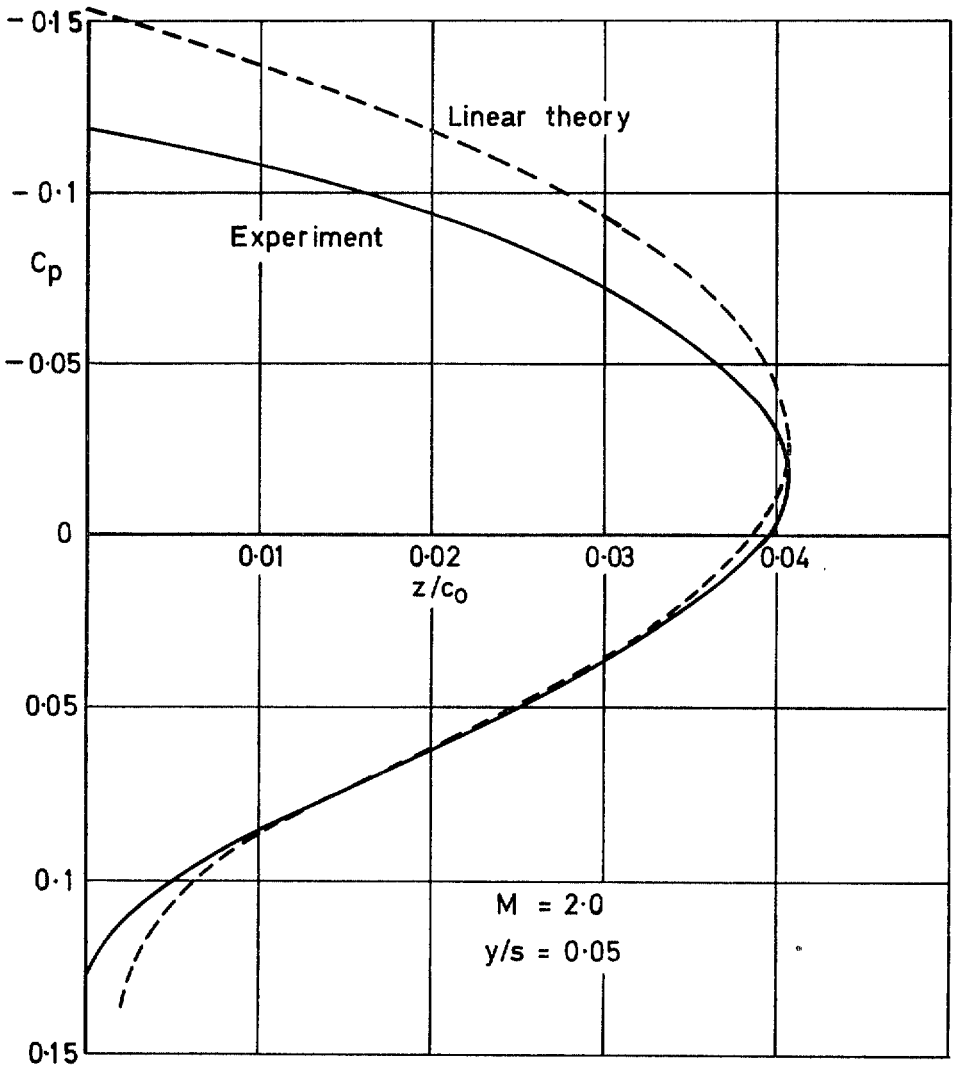

Fig.3 Chordwise pressure distribution for y/s = 0.05, model 229

Fig 4

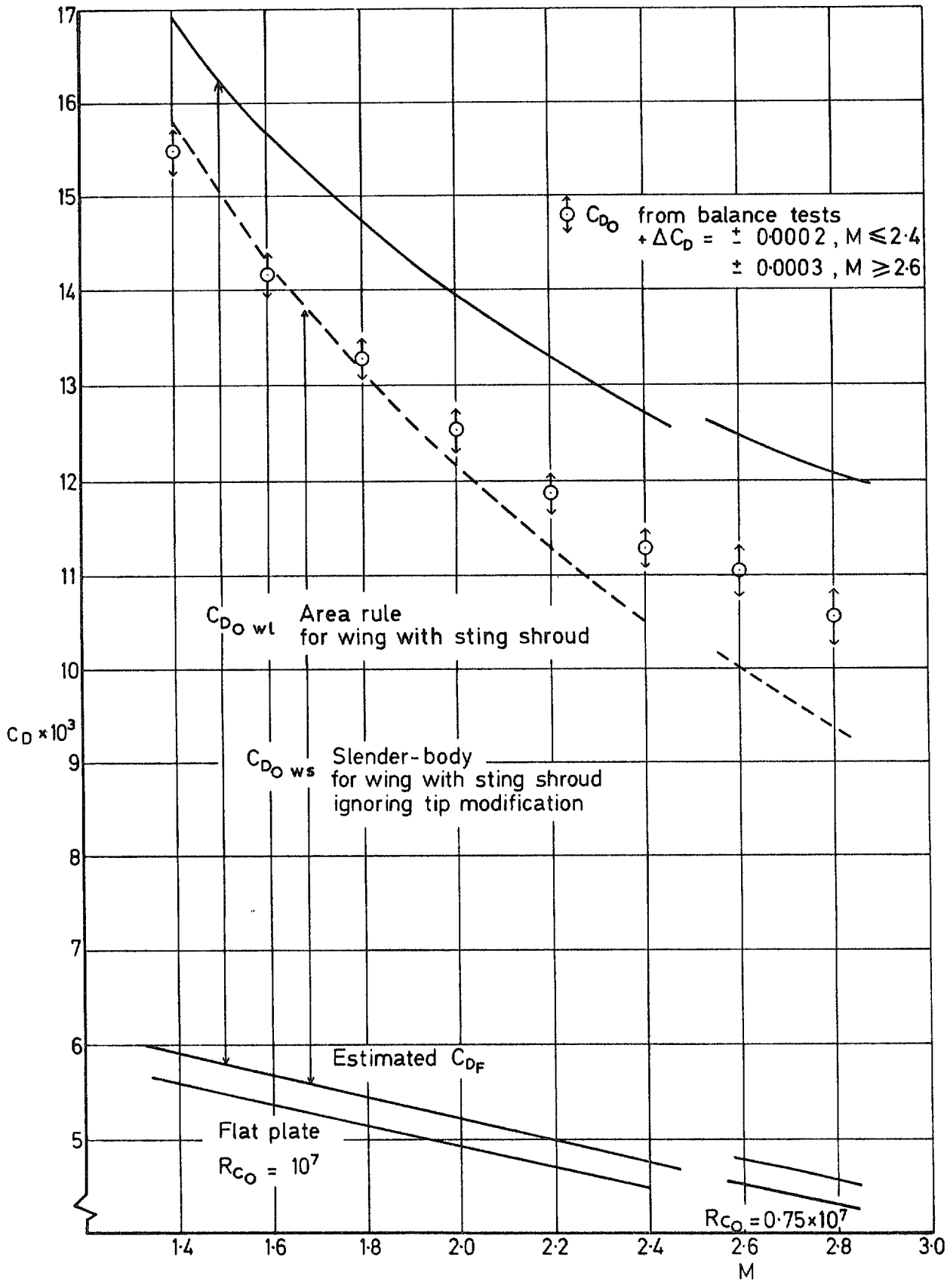

Fig.4 Zero-lift drag coefficient, model 229 with sting shroud

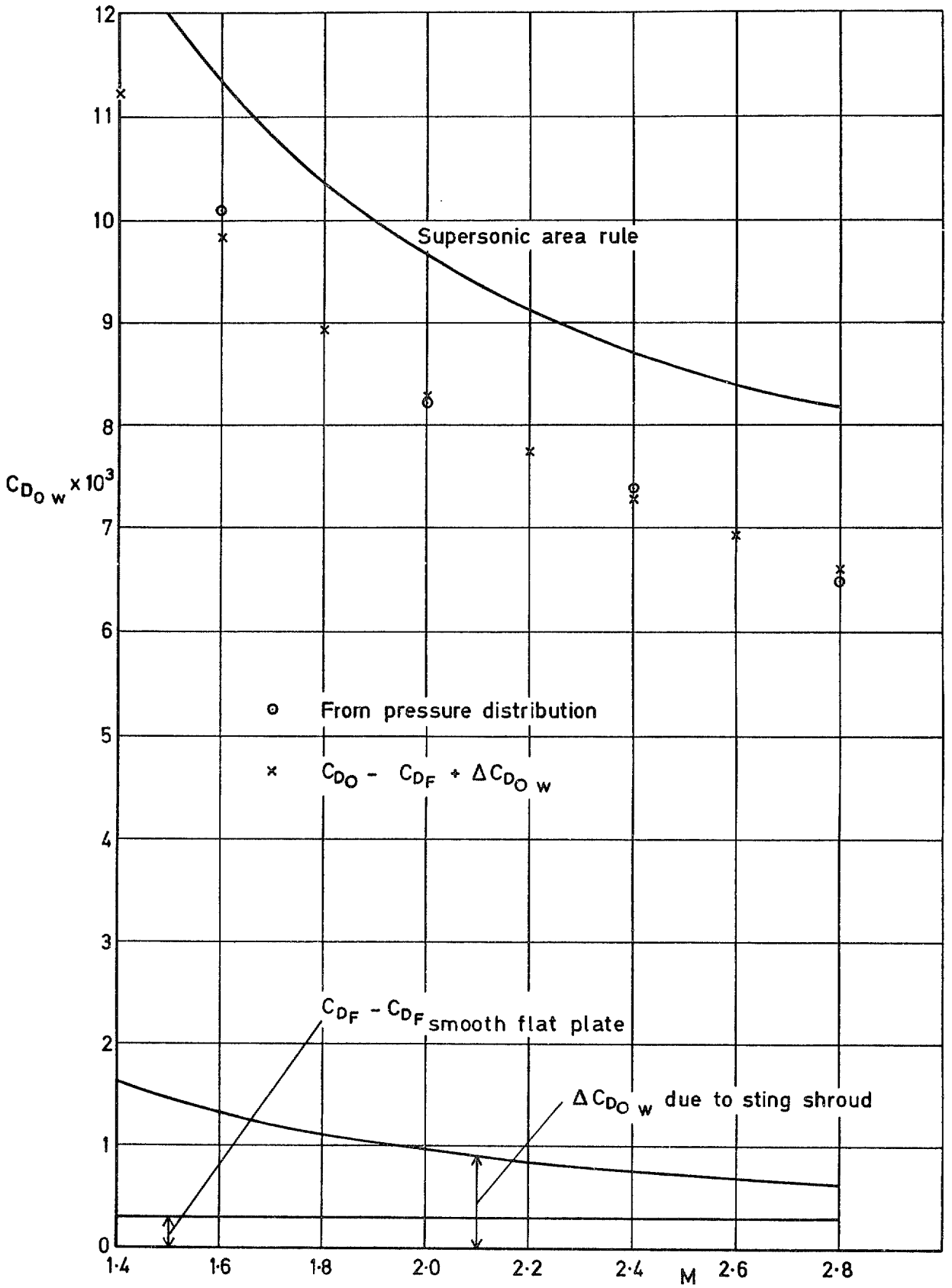

Fig.5 Comparison between the values of the zero-lift wave drag from the balance tests and from the pressure distribution; model 229 without sting shroud

Fig 6

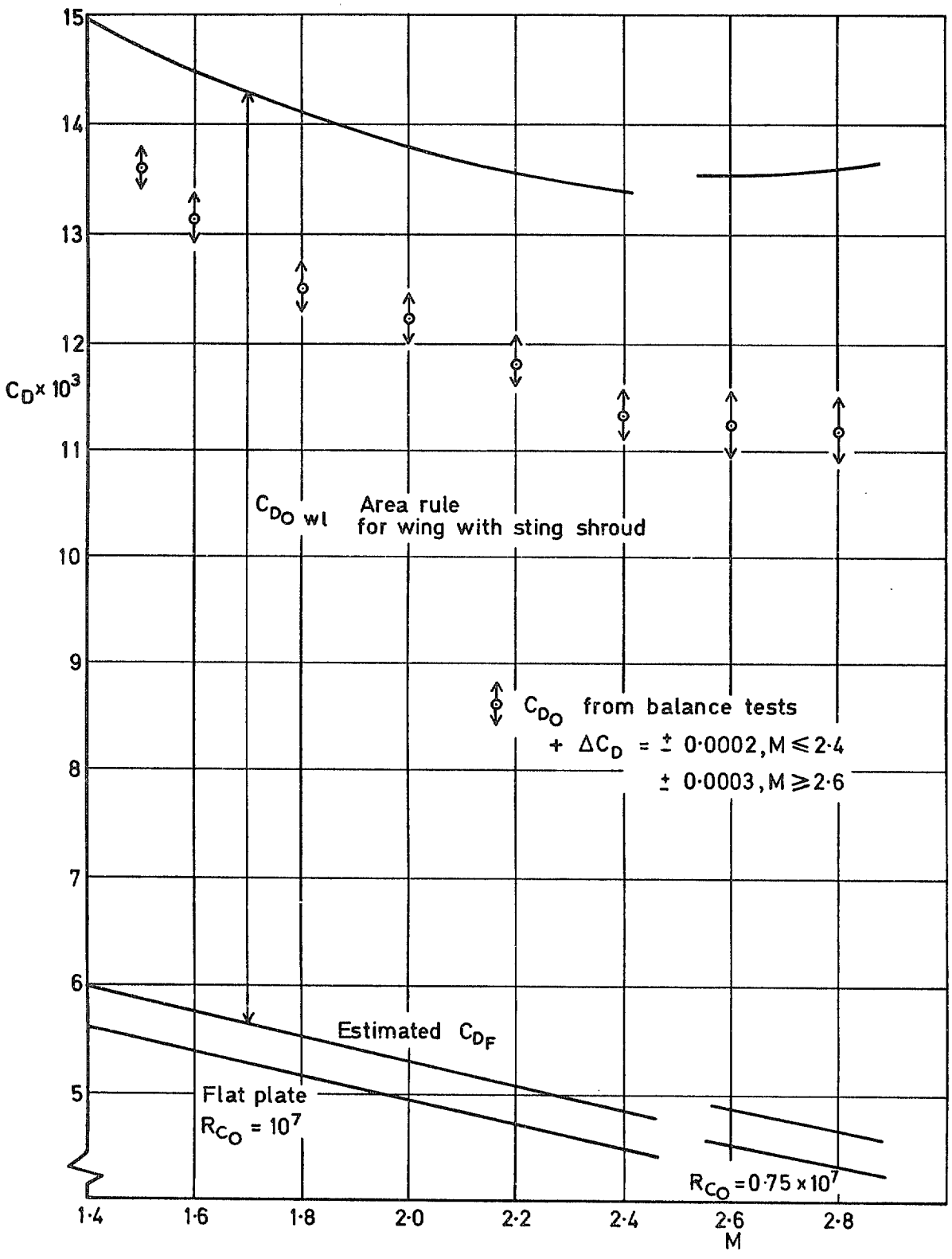

Fig.6 Zero-lift drag coefficient, model 233 with sting shroud

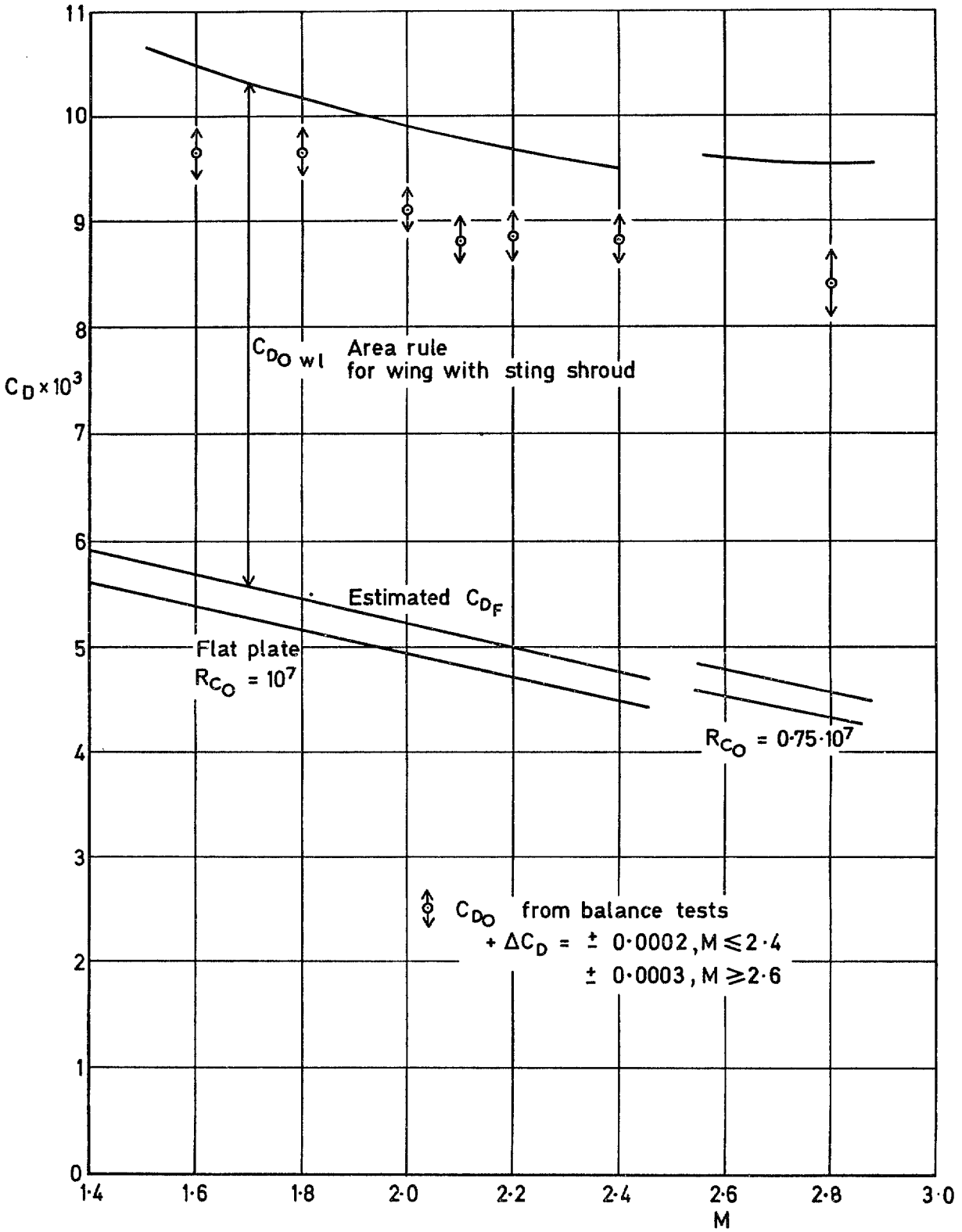

Fig.7 Zero-lift drag coefficient, model 234 with sting shroud

Fig 8

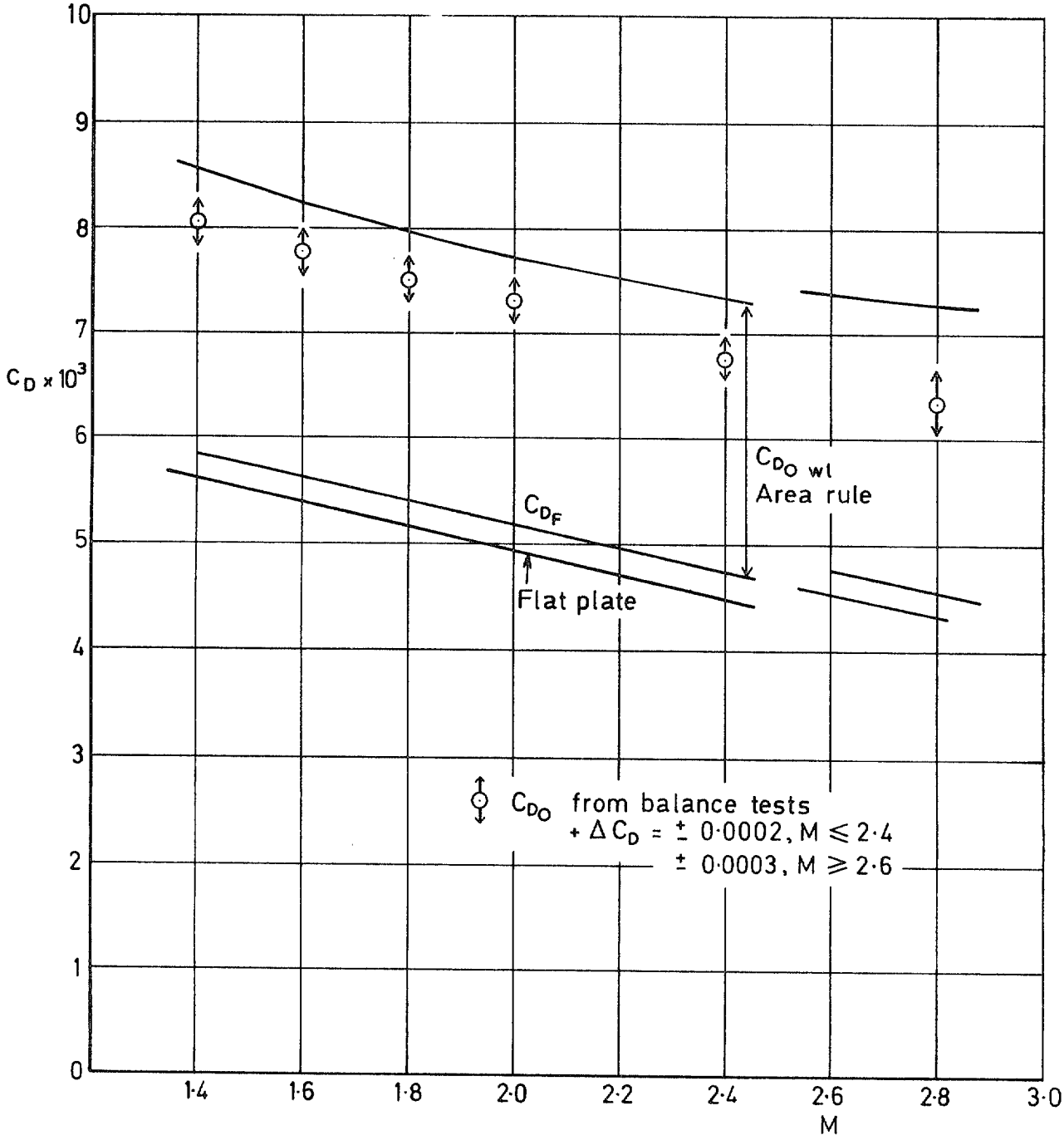

Fig.8 Zero-lift drag coefficient, model 240 with sting shroud

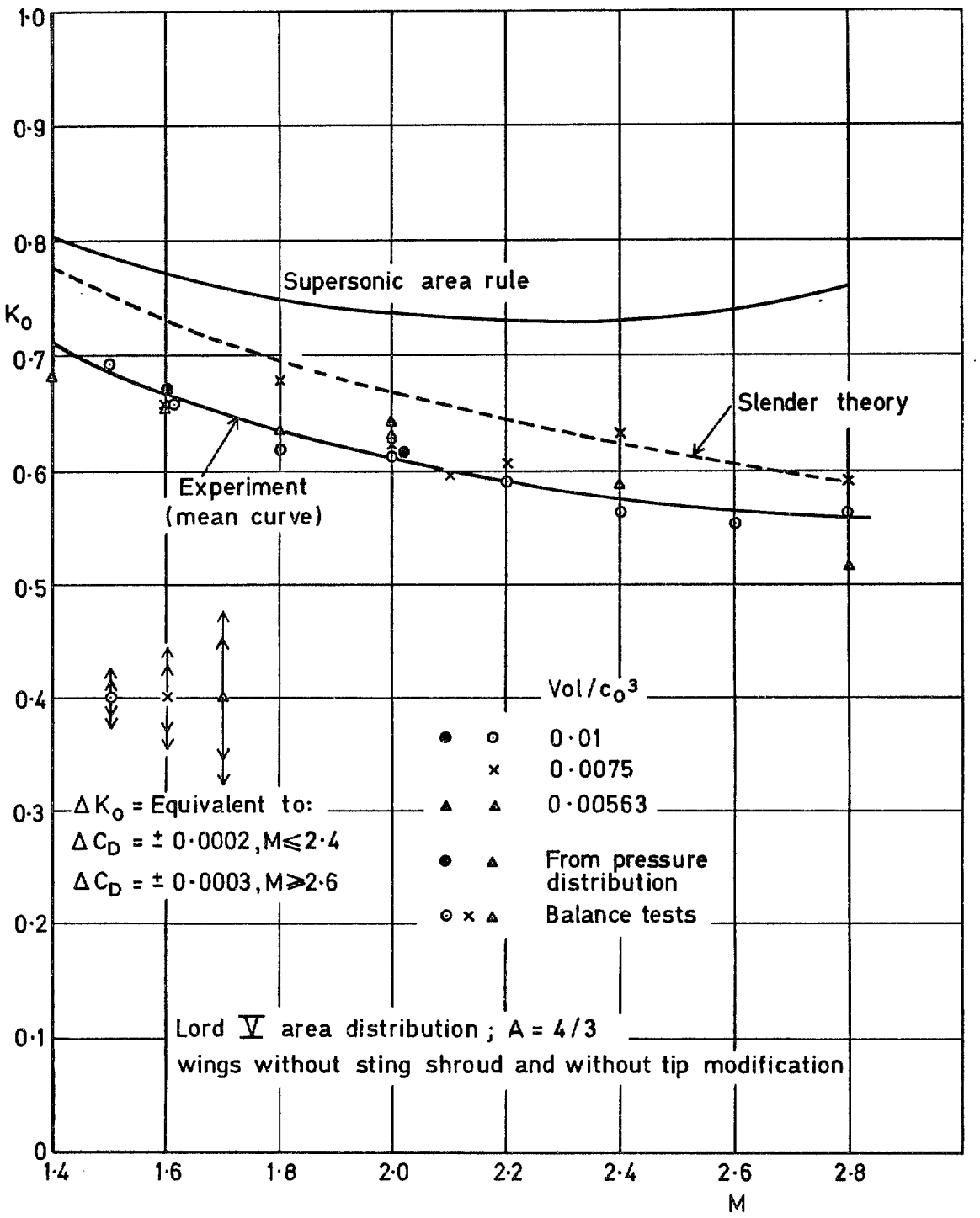

Fig.9 Zero-lift drag factor for wings of different volume

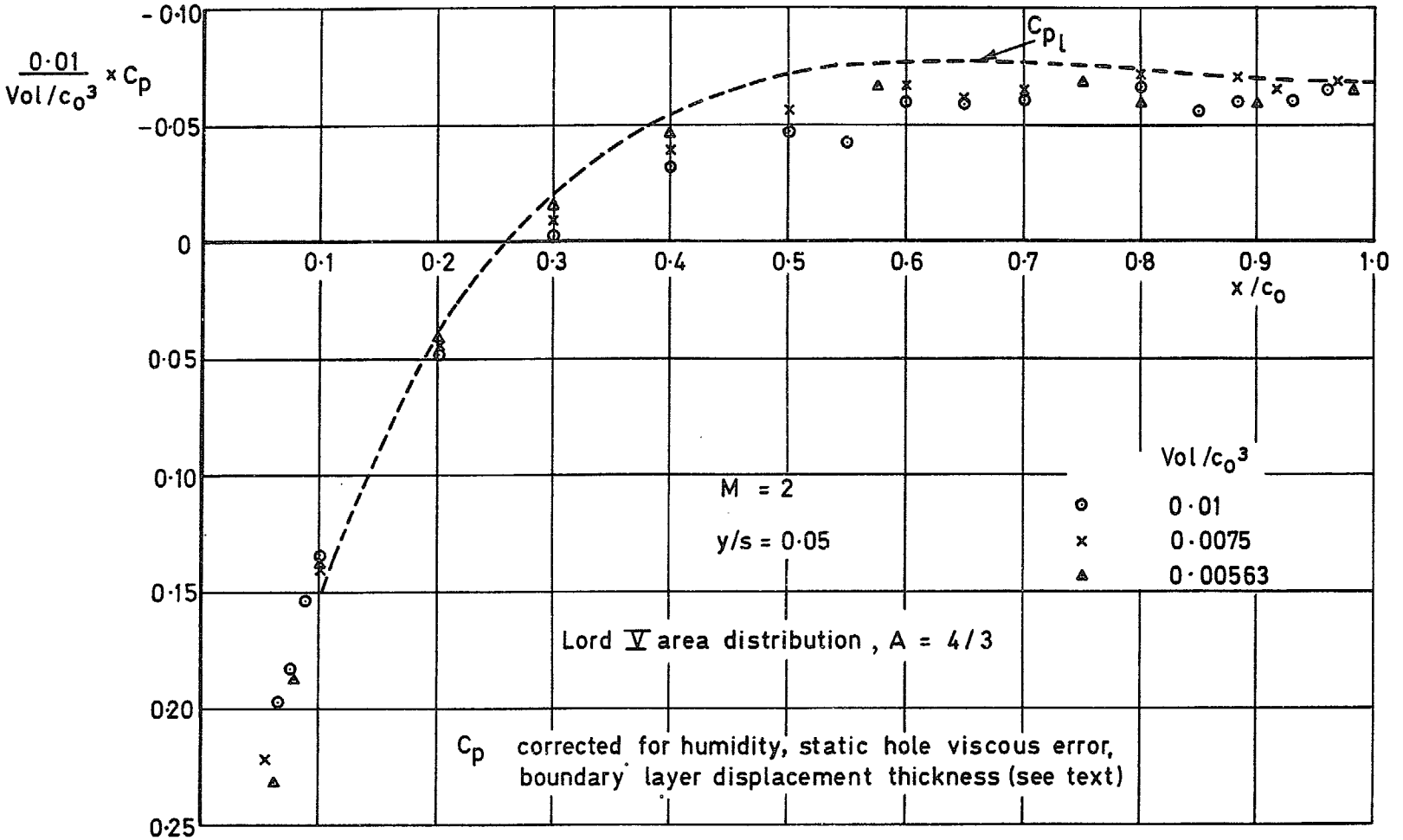

Fig.10 Chordwise pressure distribution

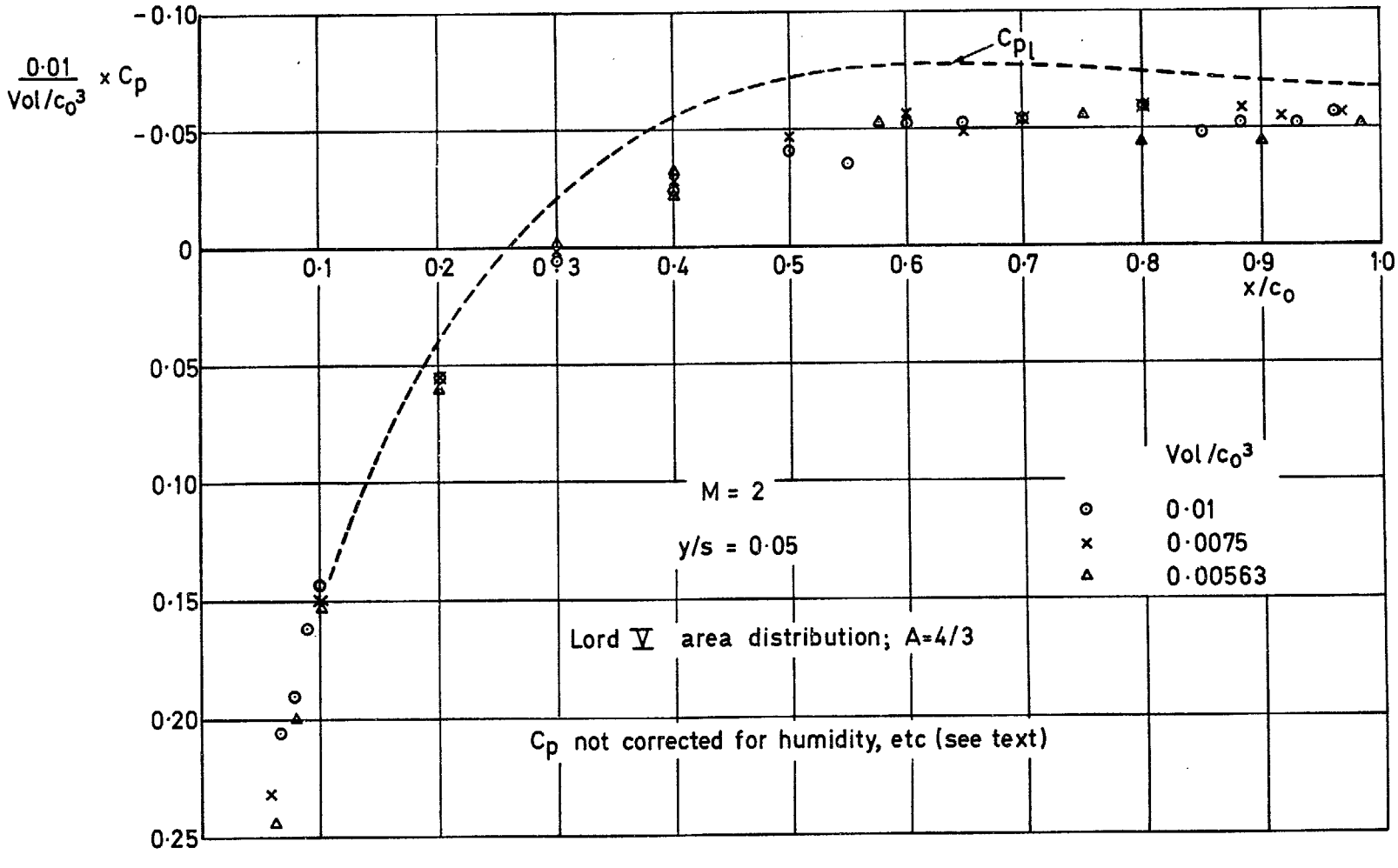

Fig.11 Chordwise pressure distribution

Fig 12

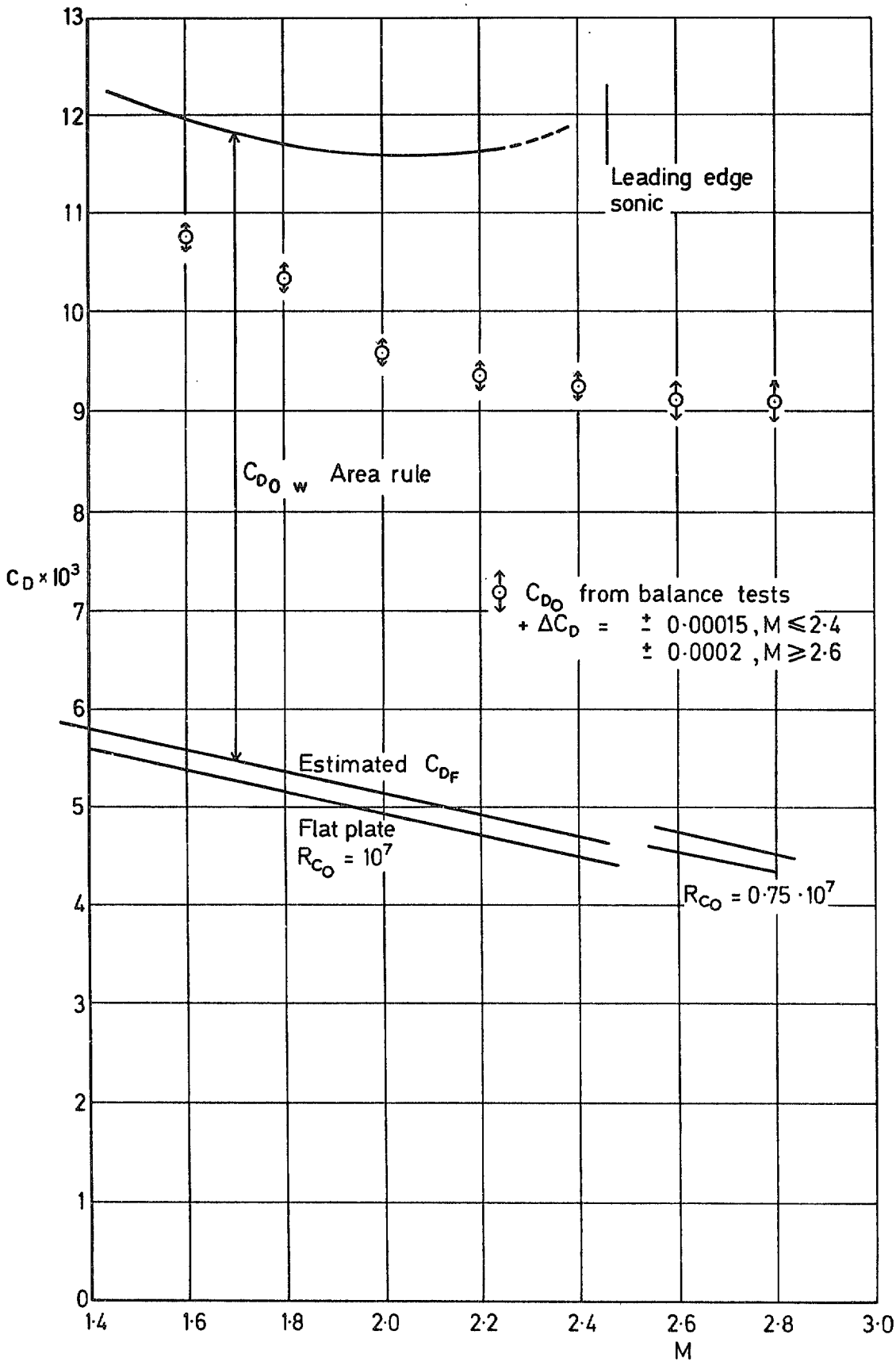

Fig.12 Zero-lift drag coefficient, model 237 with sting shroud

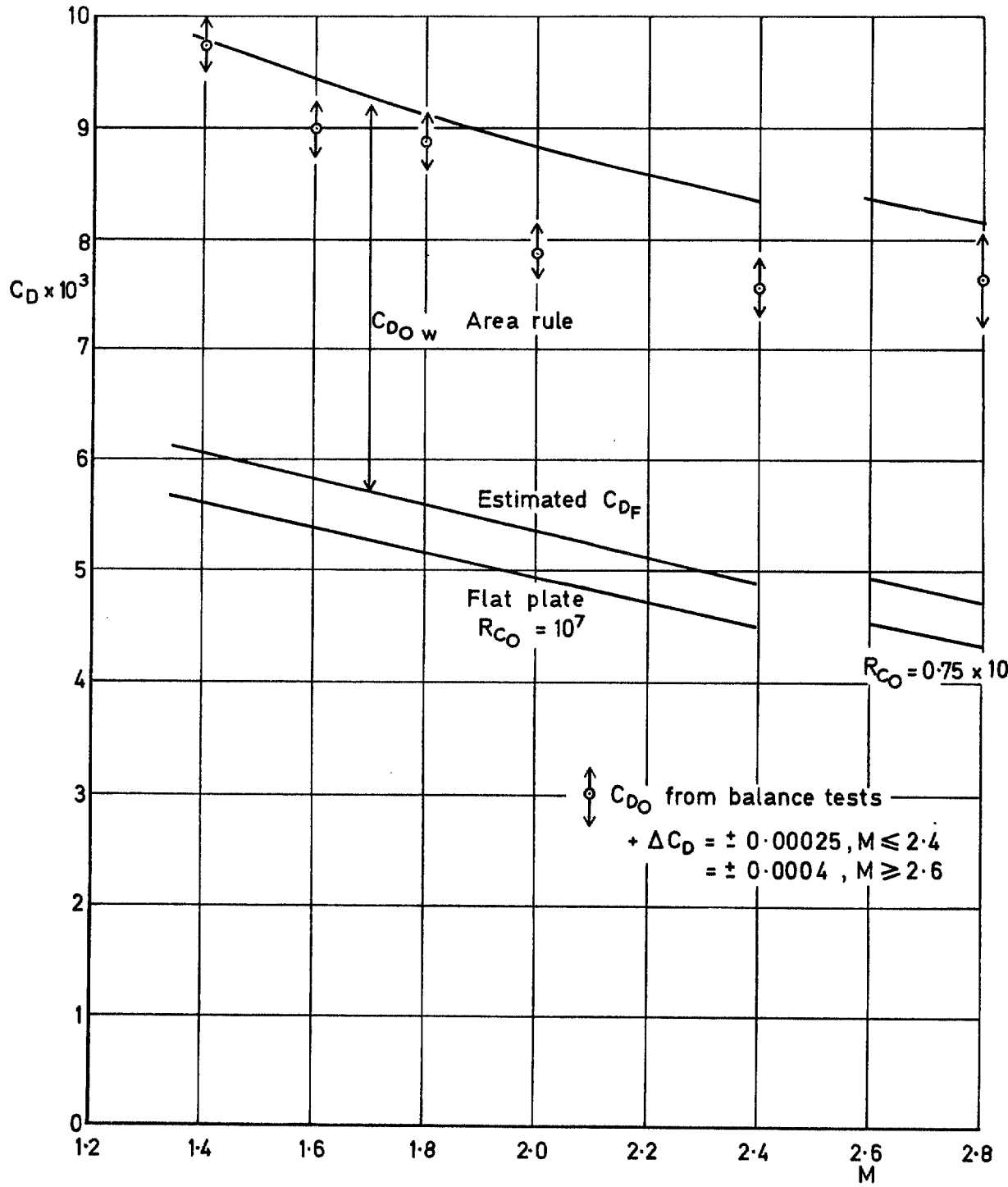

Fig.13 Zero-lift drag coefficient, model 239 with sting shroud

Fig 14

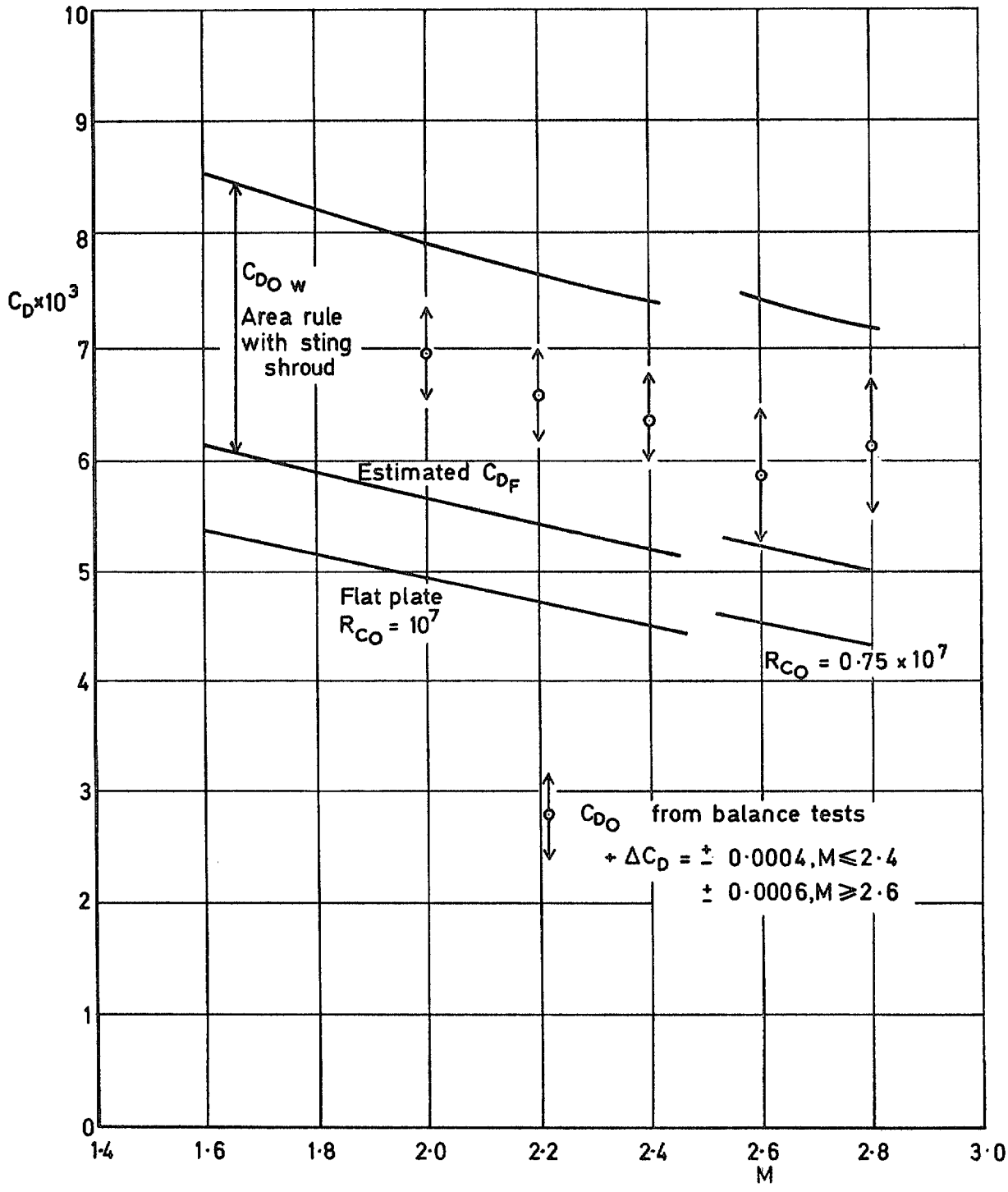

Fig.14 Zero-lift drag coefficient, model 242 with sting shroud

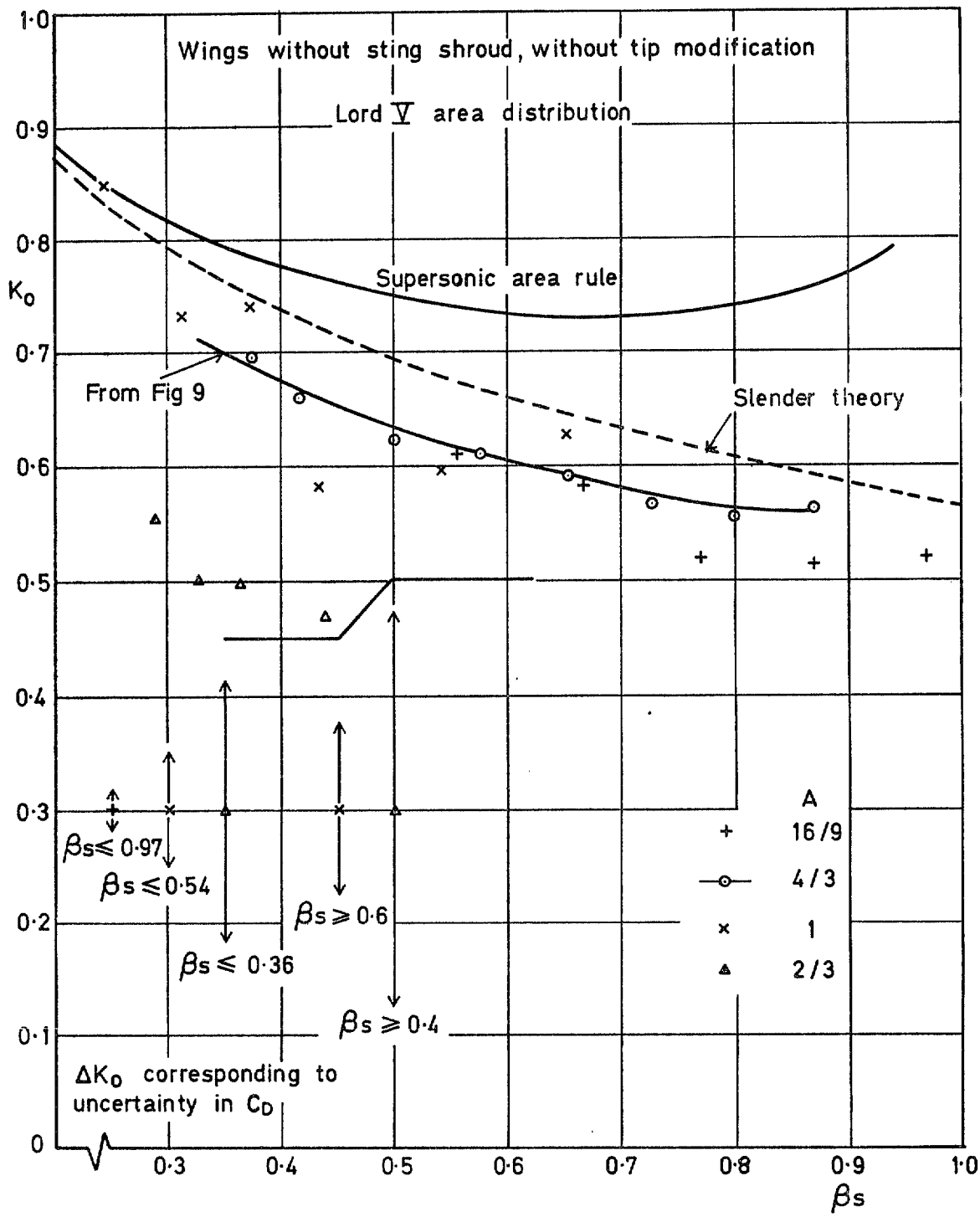

Fig.15 Zero-lift drag factor for wings of different aspect ratio

Fig 16

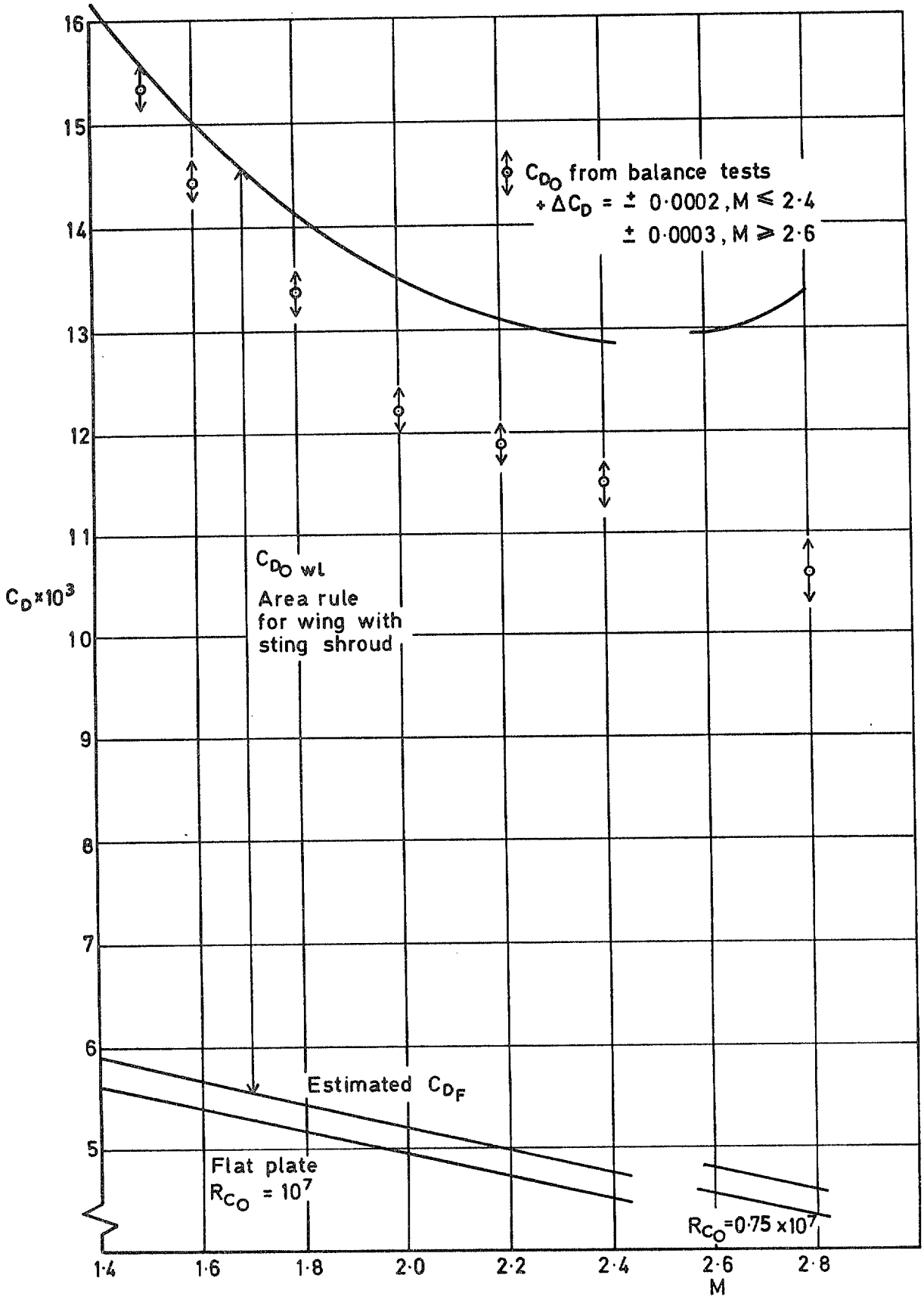

Fig.16 Zero-lift drag coefficient, model 230 with sting shroud

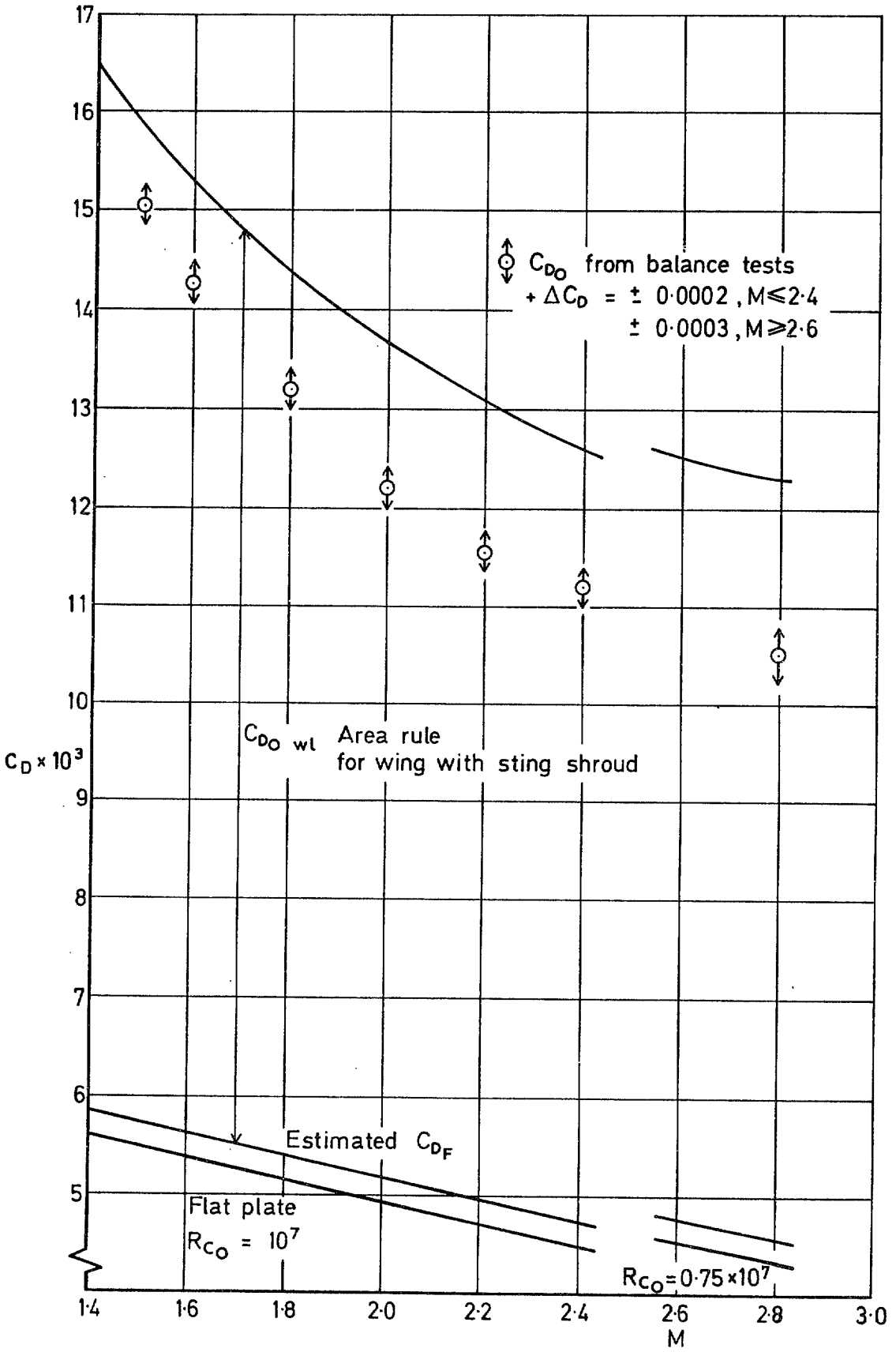

Fig. 17 Zero-lift drag coefficient, model 231 with sting shroud

Fig 18

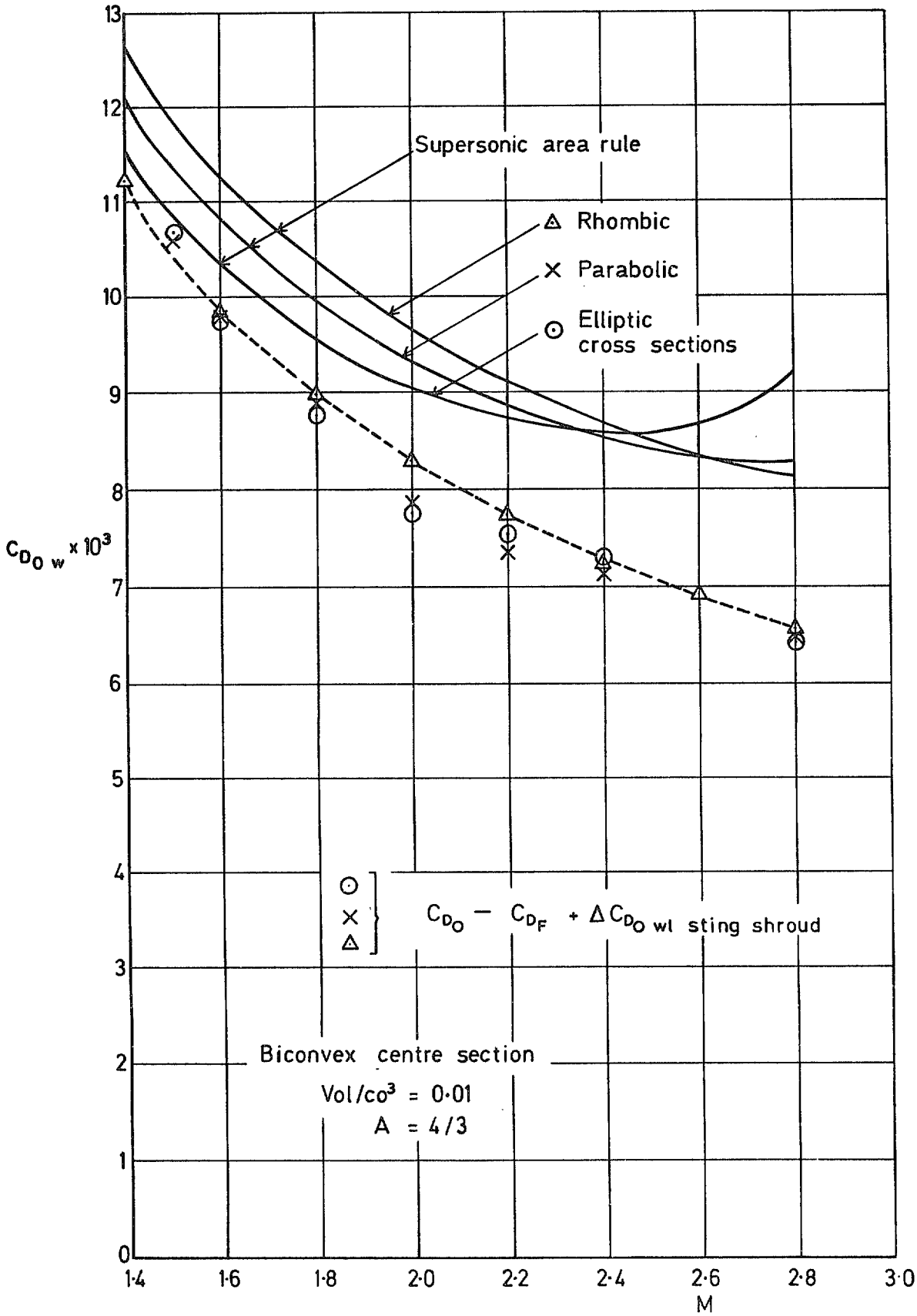

Fig.18 Zero-lift wave drag for wings of different cross-sectional shapes

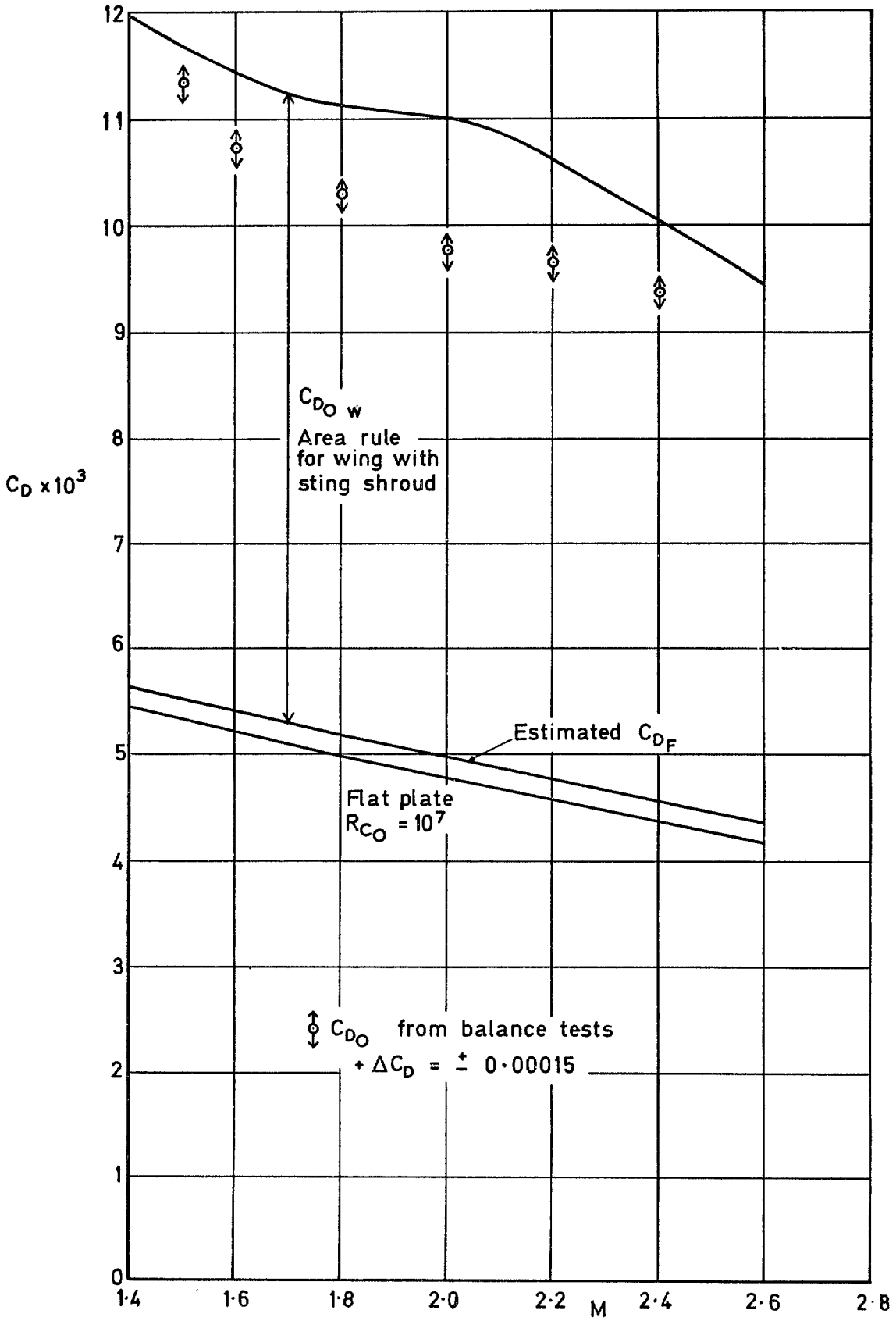

Fig.19 Zero-lift drag coefficient, model 238 with sting shroud

Fig 20

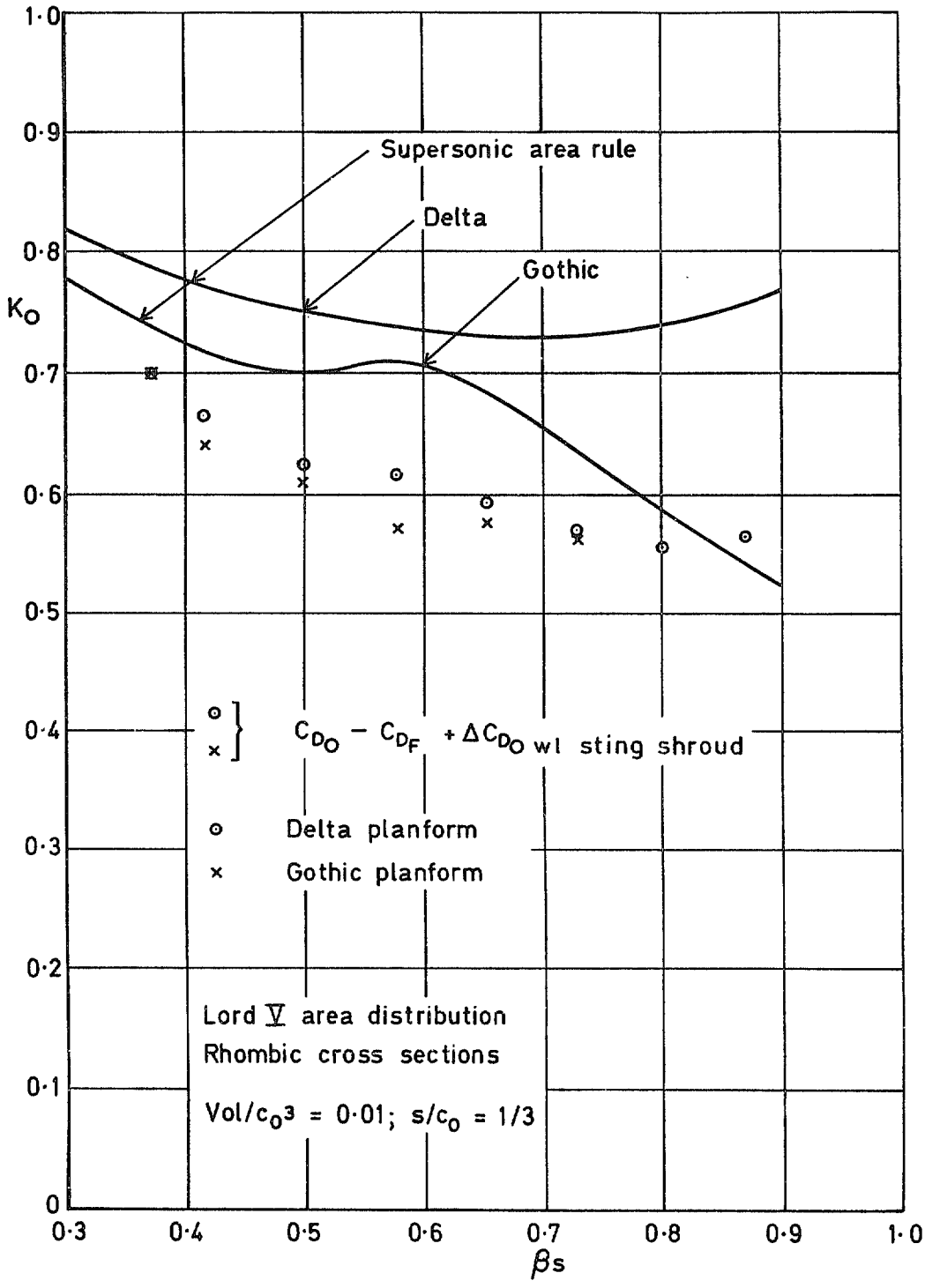

Fig.20 Zero-lift drag factor for wings of different planform

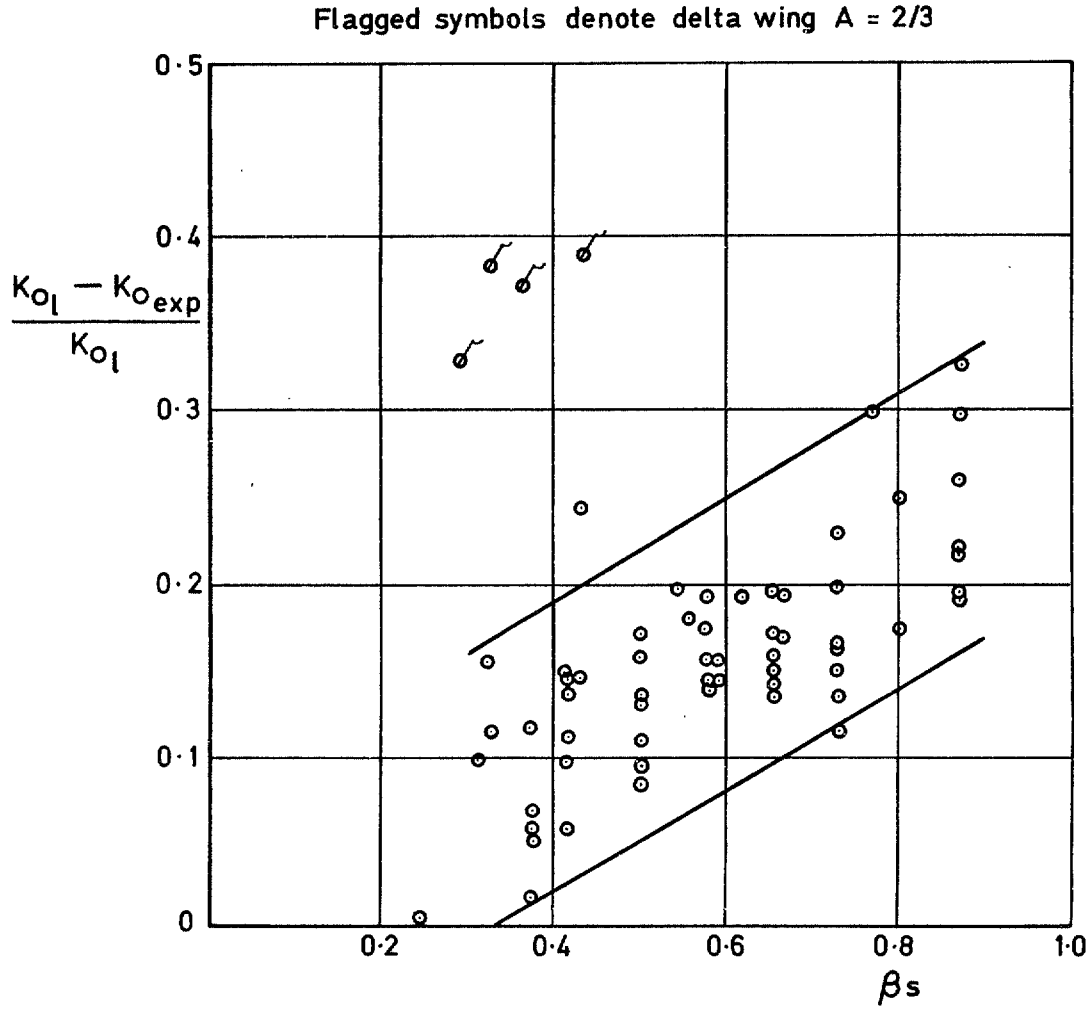

Fig.21 Error in the zero-lift wave drag derived by linear theory

Fig 22

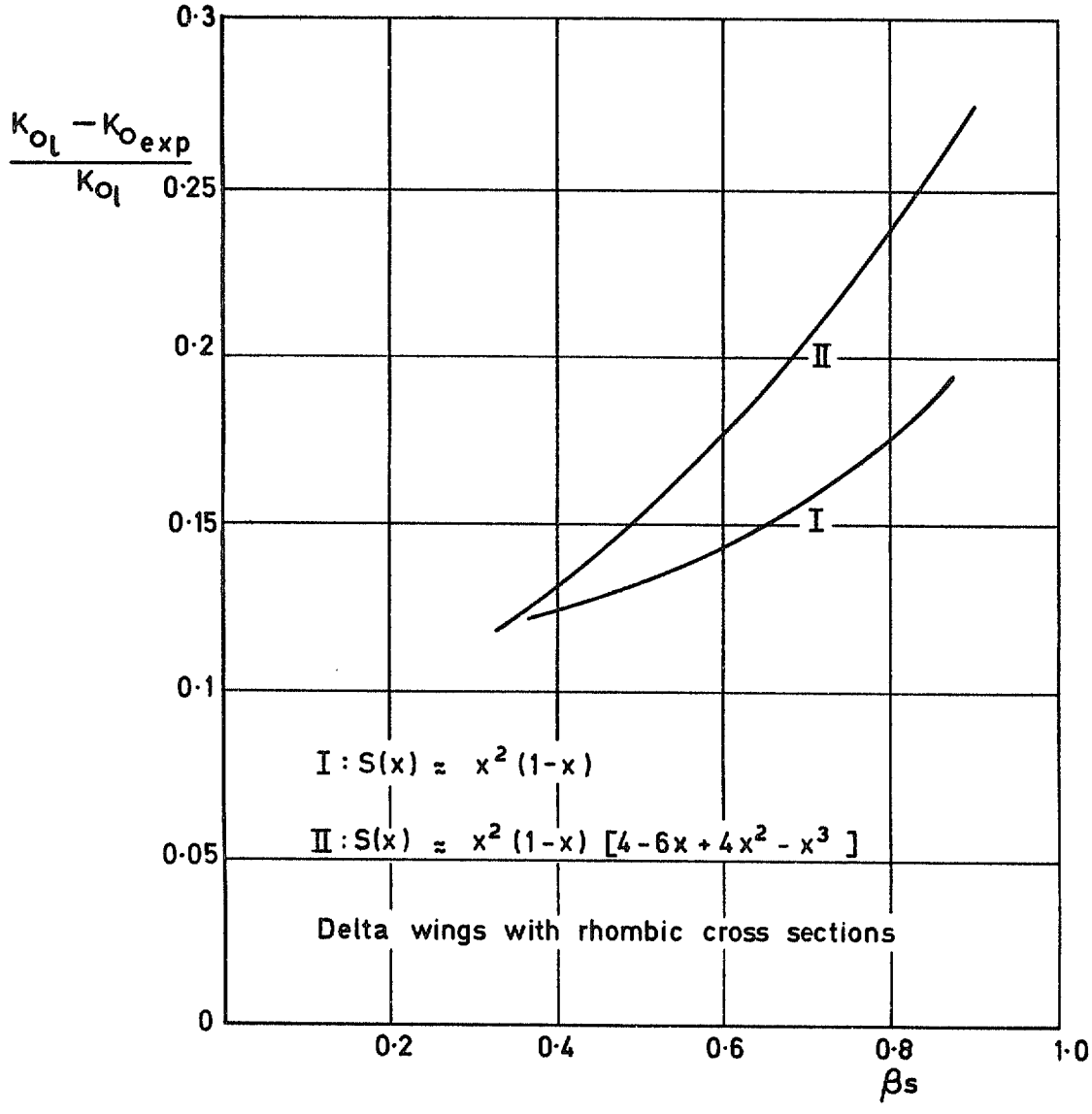

Fig.22 Error in the zero-lift wave drag derived by linear theory for delta wings with different area distributions

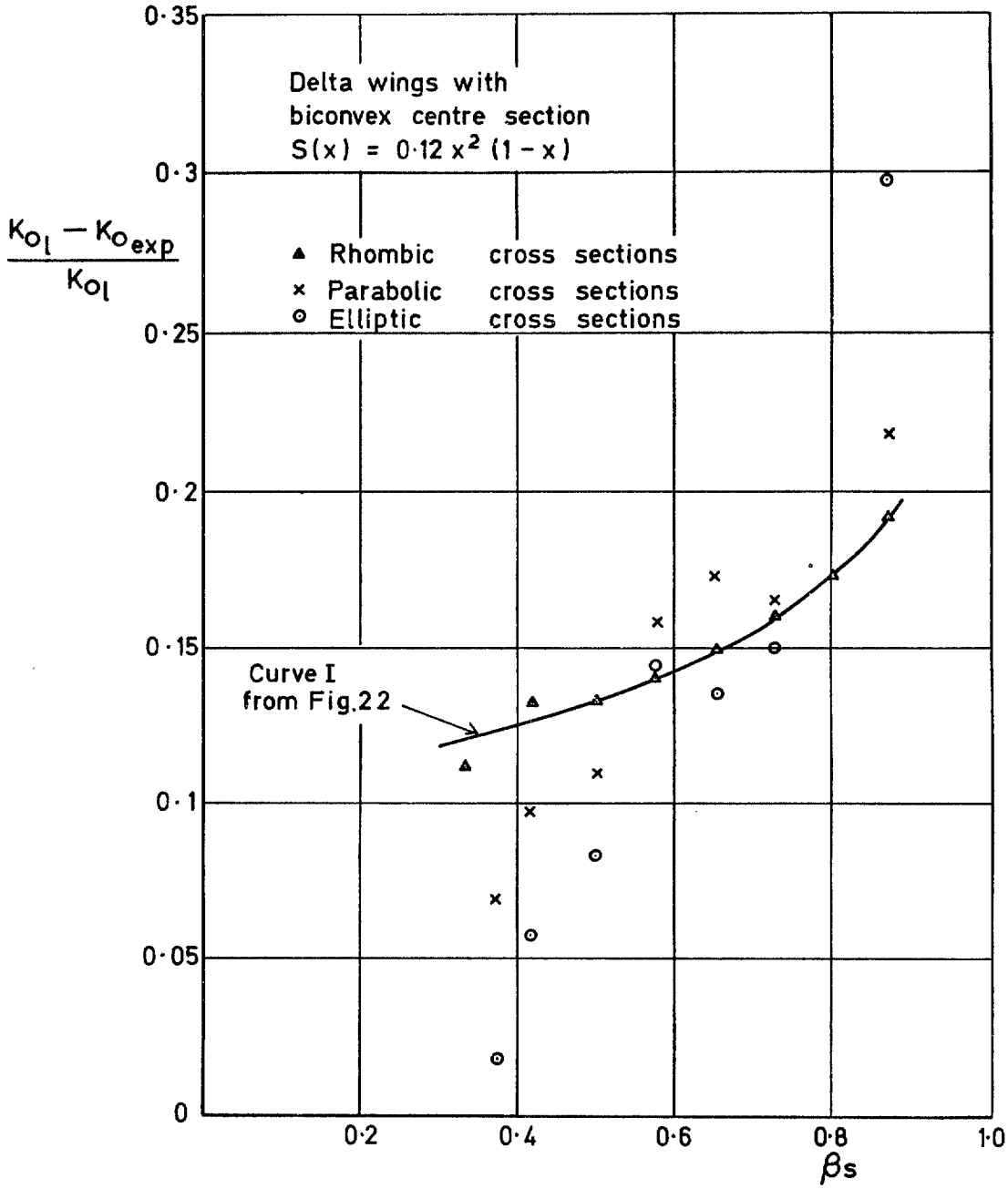

Fig 23 Error in the zero-lift wave drag derived by linear theory for delta wings with the same area distribution but different type of cross sections

Fig 24

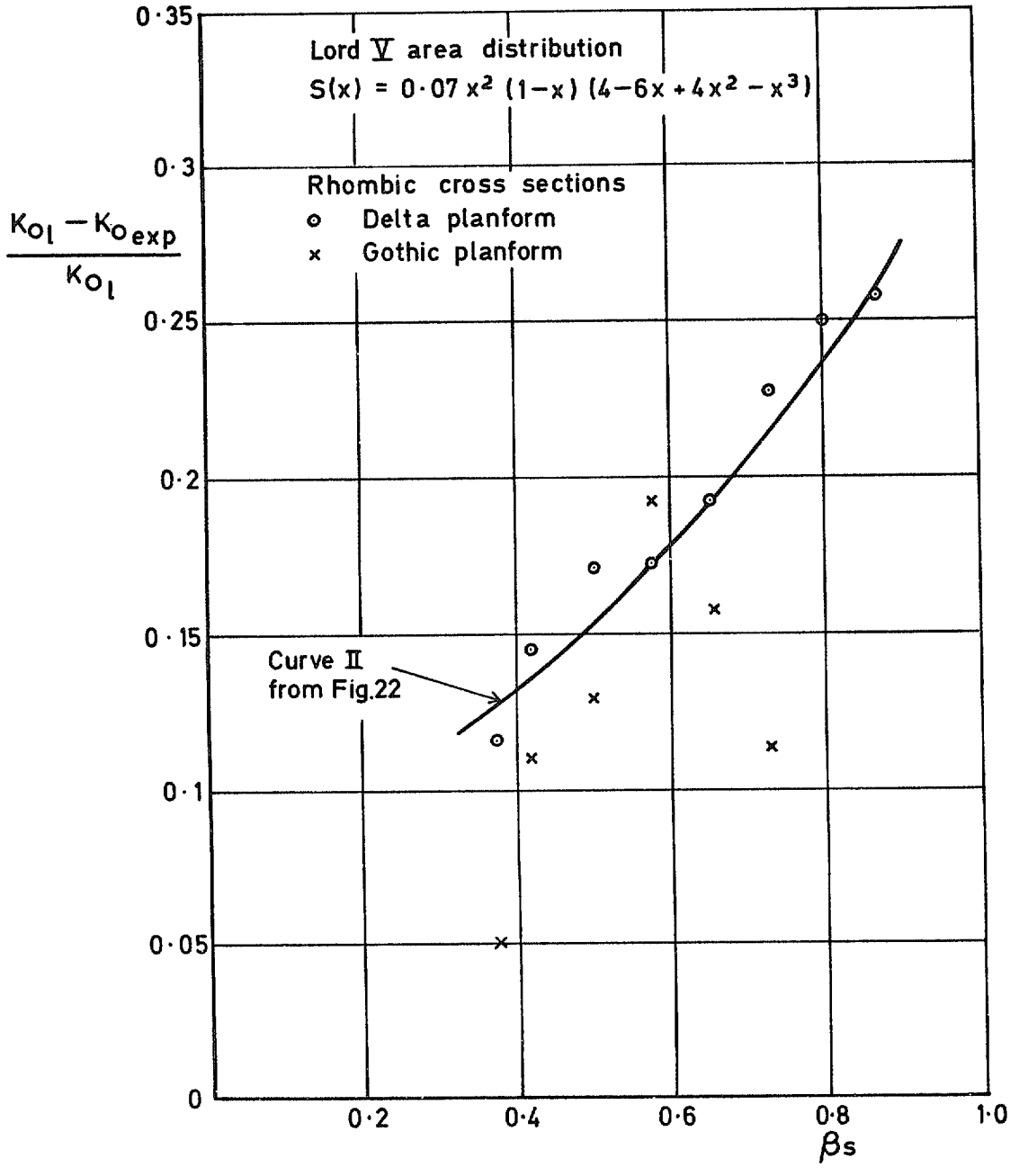

Fig.24 Error in the zero-lift wave drag derived by linear theory for wings with the same area distribution but with different planforms

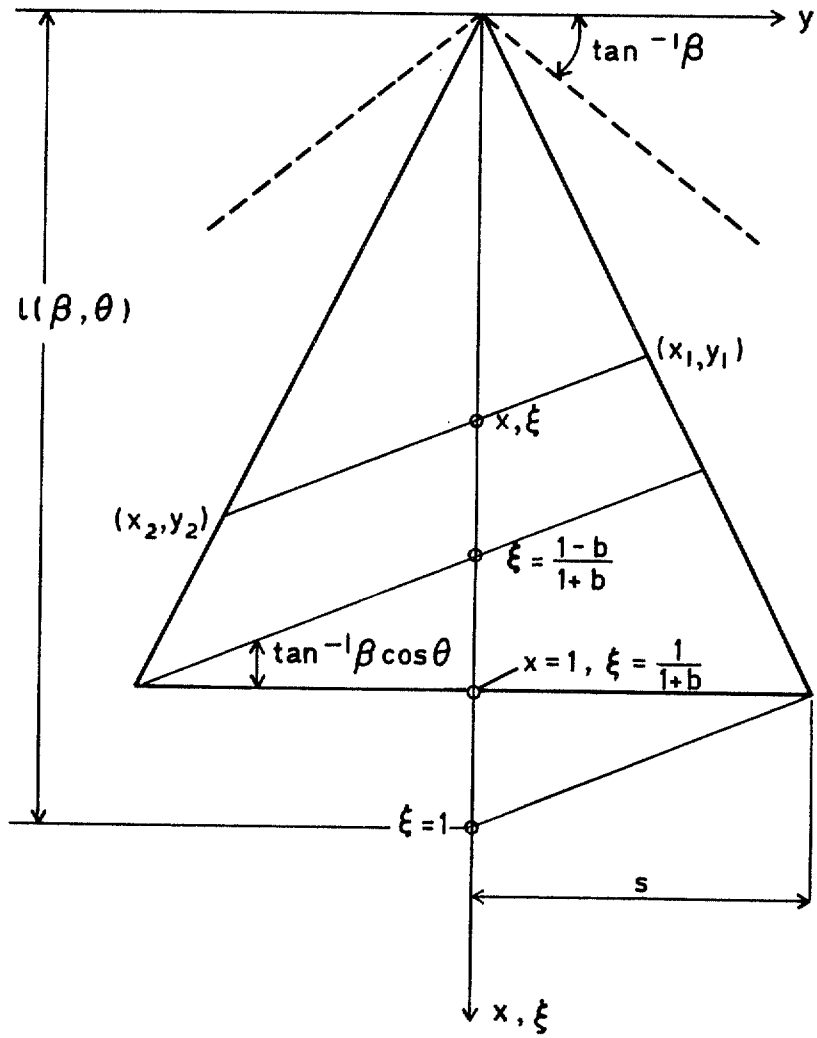

Fig.25 Notation for Appendix A

Fig 26

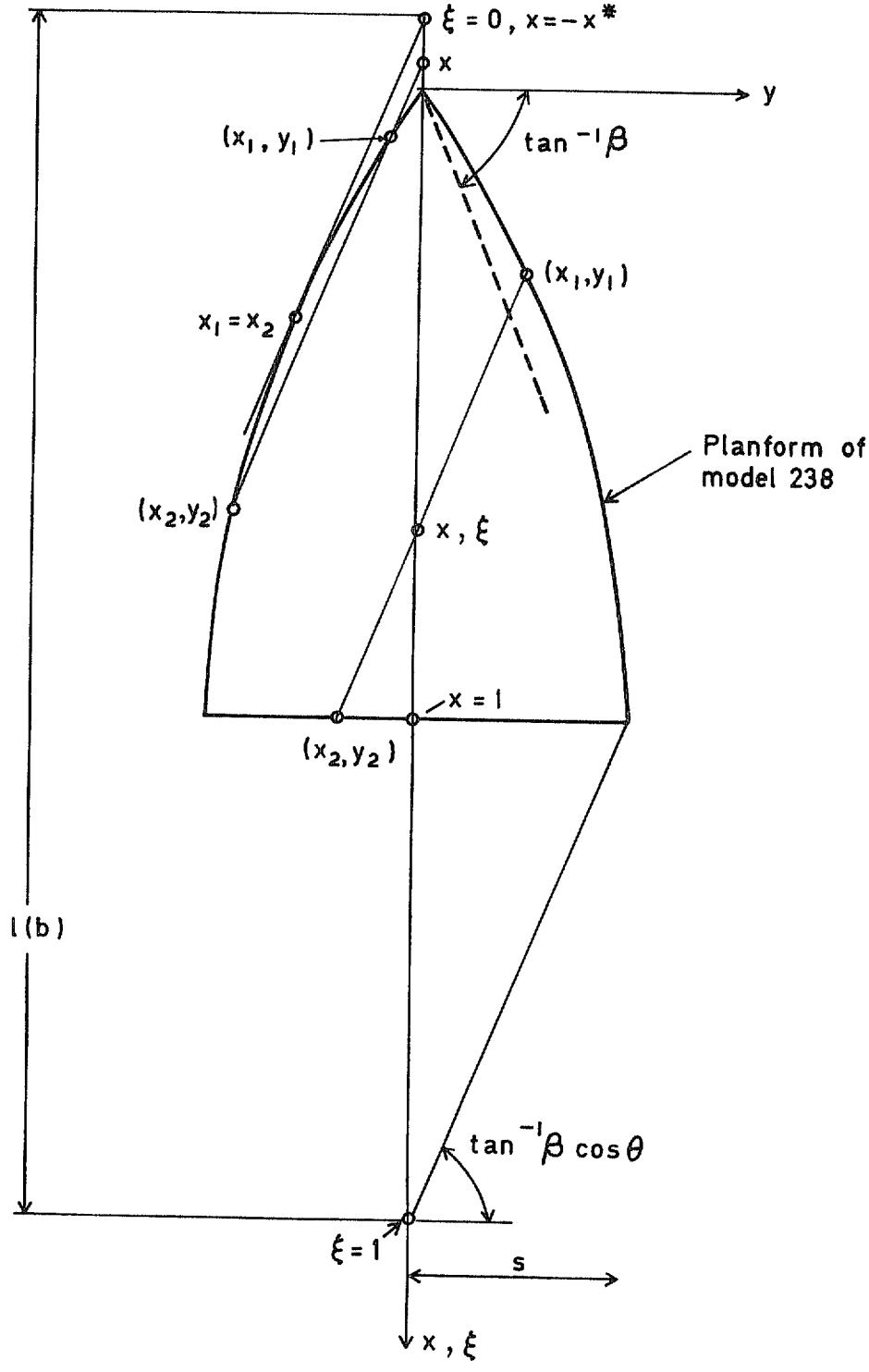

Fig.26 Notation for Appendix A

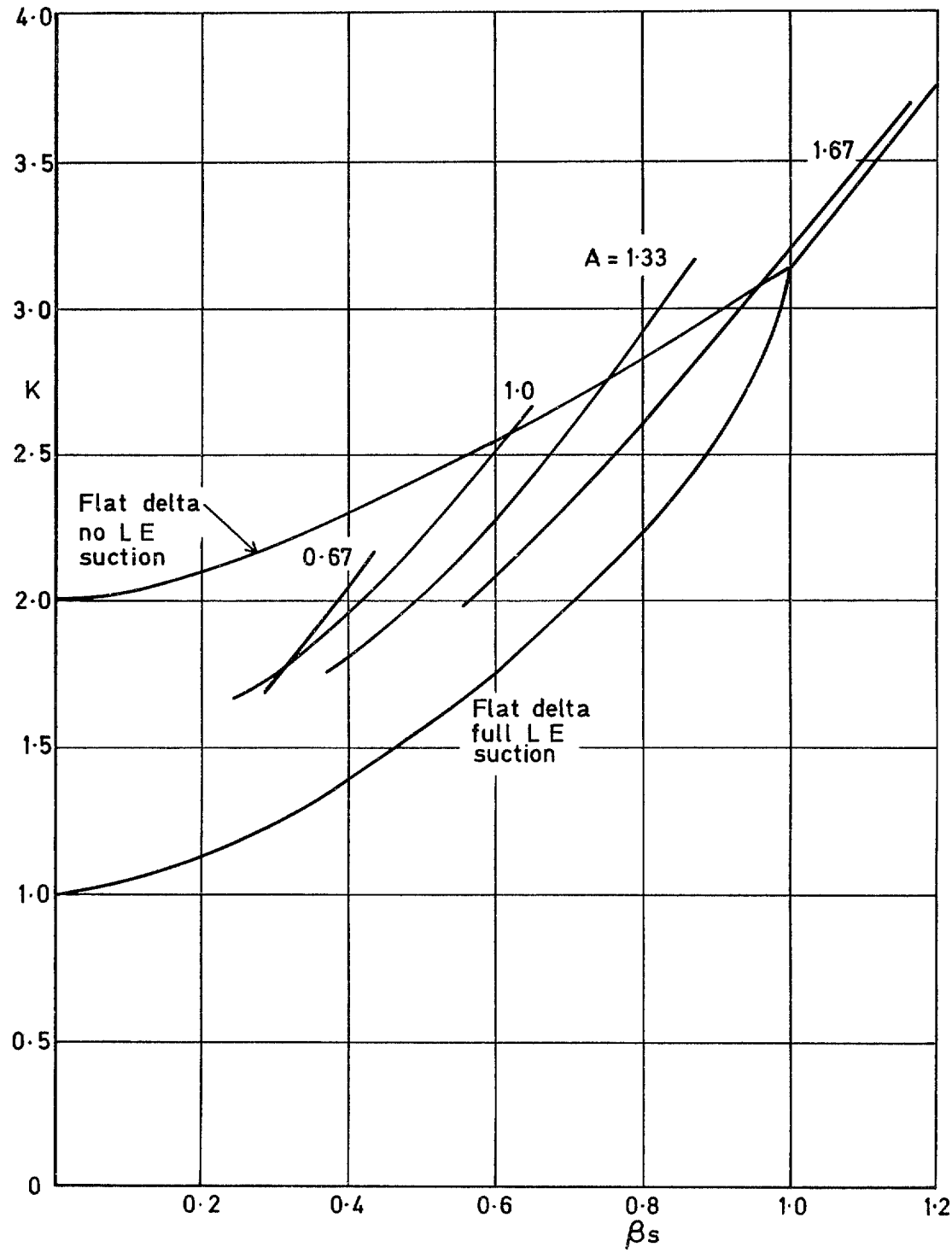

Fig.27 Lift-dependent drag factor for delta wings with rhombic cross sections at small $|C_L|$; $|\alpha| < 3°$

Fig 28

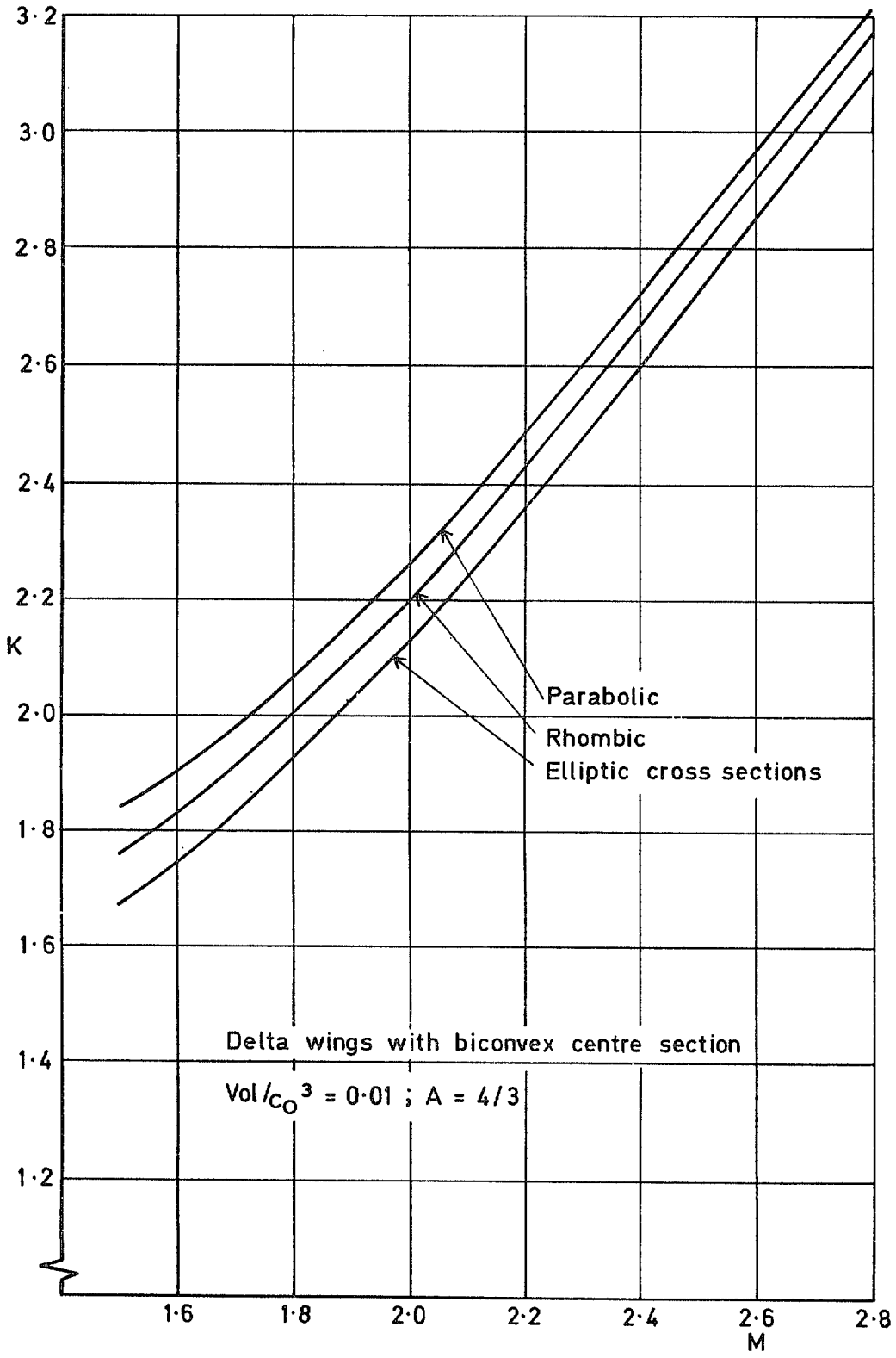

Fig.28 Lift-dependent drag factor at small $|C_L|$

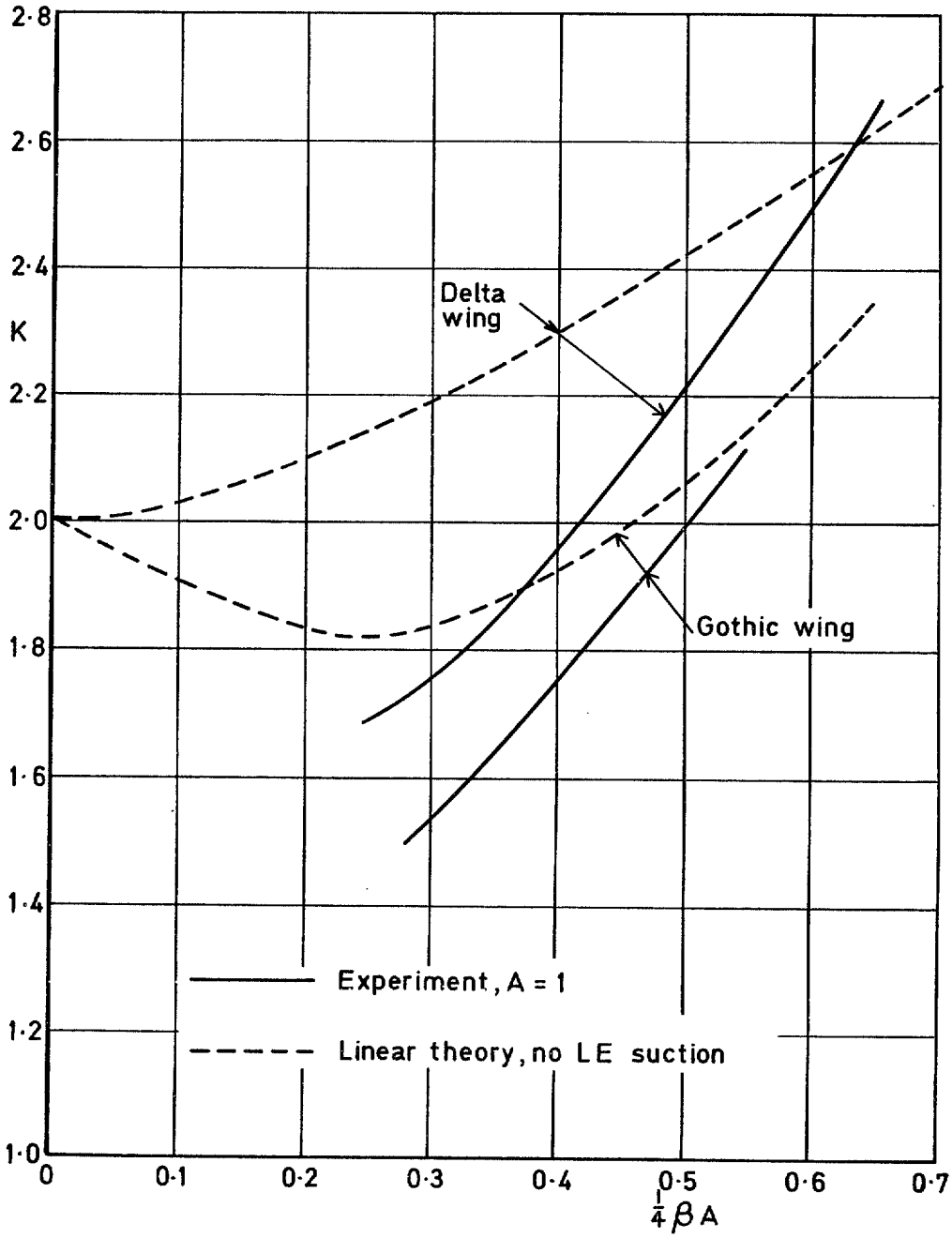

Fig.29 Lift-dependent drag factor at small $|C_L|$

Printed in England for Her Majesty's Stationery Office by the Royal Aircraft Establishment, Farnborough. Dd. 587484 K5 2/78.

Published by
HER MAJESTY'S STATIONERY OFFICE

Government Bookshops
49 High Holborn, London WC1V 6HB
13a Castle Street, Edinburgh EH2 3AR
41 The Hayes, Cardiff CF1 1JW
Brazennose Street, Manchester M60 8AS
Southey House, Wine Street, Bristol BS1 2BQ
258 Broad Street, Birmingham B1 2HE
80 Chichester Street, Belfast BT1 4JY

Government Publications are also available through booksellers

R &M No.3818
ISBN 0 11 471151 8